HHS Public Access

Author manuscript

Neuron. Author manuscript; available in PMC 2024 October 18.

Published in final edited form as:

Neuron. 2023 October 18; 111(20): 3288–3306.e4. doi:10.1016/j.neuron.2023.07.011.

Neural dynamics in the limbic system during male social behaviors

Zhichao Guo[1,2], **Luping Yin**[1], **Veronica Diaz**[1], **Bing Dai**[1], **Takuya Osakada**[1], **Julieta E. Lischinsky**[1], **Jonathan Chien**[3], **Takashi Yamaguchi**[1], **Ashley Urtecho**[1], **Xiaoyu Tong**[1], **Zhe S. Chen**[1,3,4], **Dayu Lin**[1,3,5]

[1]Neuroscience Institute, New York University Grossman School of Medicine, New York, NY, 10016, USA

[2]School of Life Sciences, Peking University, Beijing, 100871, China

[3]Department of Psychiatry, Department of Neuroscience and Physiology, New York University Grossman School of Medicine, New York, NY, USA; Center for Neural Science, New York University, New York, NY, 10016, USA

[4]Department of Biomedical Engineering, New York University Tandon School of Engineering, Brooklyn, NY 11201, USA

SUMMARY

Sexual and aggressive behaviors are vital for species survival and individual reproductive success. Although many limbic regions have been found relevant to these behaviors, how social cues are represented across regions and how the network activity generates each behavior remains elusive. To answer these questions, we utilize multi-fiber photometry (MFP) to simultaneously record Ca^{2+} signals of estrogen receptor alpha (Esr1)-expressing cells from 13 limbic regions in male mice during mating and fighting. We find that conspecific sensory information and social action signals are widely distributed in the limbic system and can be decoded from the network activity. Cross-region correlation analysis reveals striking increases in the network functional connectivity during the social action initiation phase, whereas late copulation is accompanied by a “dissociated” network state. Based on the response patterns, we propose a mating-biased network (MBN) and an aggression-biased network (ABN) for mediating male sexual and aggressive behaviors, respectively.

[5]Correspondence: Dayu.Lin@nyulangone.org (D.L.).
Lead contact: Dayu.Lin@nyulangone.org (D.L.)

AUTHOR CONTRIBUTIONS

D.L conceived and supervised the project, designed experiments, analyzed the data, and wrote the manuscript. Z.G. conducted most experiments, performed preliminary data analyses, and wrote an earlier draft. L.Y. performed some MFP recordings and data analysis during the paper revision. V. D. designed and performed the behavioral experiment in Figure S11. B.D. and X.T. performed animal tracking. B.D., T.O., J.E.L., and T.Y. performed preliminary recording and behavior experiments. A.U. assisted with behavior annotation. J.C. assisted data analysis under the supervision of Z.S.C.

DECLARATION OF INTERESTS

The authors declare no competing interests.

eTOC Blurb

Guo et al. use multi-fiber photometry to simultaneously record Ca^{2+} activity from 13 brain regions in the expanded social behavior network during mating and fighting in male mice. The recording reveals widespread activities in the network that evolve in distinct ways throughout male-male and male-female social interactions.

INTRODUCTION

Sexual and aggressive behaviors are fundamental to animal survival and reproduction. These behaviors are innate, i.e., inborn, and thus, their generation should be supported by hardwired circuits. In 1999, Sarah Newman proposed the existence of a social behavior network (SBN) that mediates innate social behaviors in mammals based on decades of lesion and immediate early gene mapping studies[1]. The SBN includes seven interconnected subcortical areas: the medial amygdala (MeA), bed nucleus of stria terminalis (BNST), medial preoptic area (MPOA), anterior hypothalamus (AHN), lateral septum (LS), ventromedial hypothalamus (VMH), and midbrain (including periaqueductal gray (PAG) and tegmentum)[1]. MeA and BNST are collectively called the extended medial amygdala. In 2005, James Goodson extended this network to non-mammalian vertebrate species based on studies in birds and teleost (bony) fish[2]. In recent years, the importance of SBN in social behaviors has been continuously validated and elaborated. For instance, gain- and loss-of-function studies demonstrated indispensable roles of the ventrolateral part of the VMH (VMHvl) and MeA in aggressive behaviors in mice[3–14], while the molecular identities of cells in the medial preoptic nucleus (MPN) relevant for sexual behaviors have been increasingly refined[15–18]. As to BNST, several recent studies revealed its functional role in both male sexual and aggressive behaviors[19–22].

A basic feature of the SBN is its enrichment of gonadal hormone receptors, which allow the cells to be modulated by gonadal steroid hormones, including androgens (testosterone), estrogens, and progesterone[1]. Indeed, gonadal hormones are crucial for the emergence of social behaviors during development and their maintenance during adulthood in both sexes[23,24]. For example, female mice exposed to prenatal testosterone show male-like sexual and aggressive behaviors during adulthood[25]. Adult castration abolishes masculine behaviors, which can be restored by testosterone supplements[26]. In males, testosterone mainly acts through estrogen receptors after being converted into estrogen via the enzyme aromatase[24]. Knocking out estrogen receptor alpha (Esr1) disrupts male sexual and aggressive behaviors severely[27–29]. Thus, it is perhaps not a coincidence that Esr1-expressing cells in the MPN and VMHvl are the relevant populations for sexual and aggressive behaviors[3,4,6,7,15,16].

The SBN does not cover all regions essential for social behaviors and requires an expansion. Several regions outside the SBN have recently been identified as necessary for male sexual behaviors, aggression, or both. Posterior amygdala (PA) cells promote aggressive and sexual behaviors through projections to the VMHvl and MPN, respectively[30–32]. The ventral part of the premammillary nucleus (PMv), a hypothalamic nucleus posterior to the VMHvl, projects heavily to both MPN and VMHvl and is important for male aggression[33–35]. The

ventral subiculum (SUBv) can bi-directionally modulate aggression, at least partly through its VMHvl projection[36]. Interestingly, these newly identified social behavior-relevant regions share the same features of the original SBN: high levels of sex hormone receptor expression and extensive connections with regions in the SBN[31,37–39].

Every behavior is a phenotypical manifestation of some well-orchestrated network activity. As more behaviorally relevant regions are discovered, an important next step is to holistically understand the neural activity in an extensive network of interacting regions during social behaviors. Indeed, several recent studies attempted to achieve this goal in other behavioral contexts using large-scale single-unit recording with multi-site silicon probes, e.g., Neuropixels[40–44]. However, recording sites of silicon probes are generally distributed along the vertical shafts, making them unsuitable for simultaneous recording from multiple deep subcortical regions. As an alternative approach, fiber photometry, a method first developed to record bulk fluorescence signals from subcortical regions[45,46], has been scaled up to record from multiple regions[47,48]. Here, the lack of cellular resolution is offset by the ability to record from molecularly defined subpopulations, or in other words, cells with potentially similar functions and relatively homogeneous responses[49]. The recent incorporation of highdensity customizable multi-fiber arrays dramatically reduces the weight of the implant and associated brain damage, making it well-suited for recording multiple sites in the SBN and beyond in freely moving animals[50].

Leveraging this multi-fiber photometry (MFP) technique, we simultaneously recorded the Ca^{2+} activities of Esr1-expressing cells from 13 regions in the limbic system, referred to here as the expanded SBN, during sexual and aggressive behaviors in male mice. Our results revealed dynamic neural response patterns during mating and fighting at the network level.

RESULTS

Simultaneous recording from 13 brain regions in the expanded SBN

We selected 13 brain regions that have either been implicated in aggressive and/or sexual behaviors or are strongly connected with those regions for Ca^{2+} recording. The list includes five hypothalamic regions – medial preoptic nucleus (MPN), AHN, VMHvl, dorsomedial hypothalamus (DMH) and PMv, five amygdala regions –anterior MeA (MeAa), posterodorsal MeA (MeApd), PA, posteromedial cortical amygdala (CoApm) and posteromedial BNST (BNSTpm), and three regions outside of amygdala and hypothalamus – ventral LS (LSv), SUBv and lateral PAG (lPAG) (Figures 1A, S1)[1,3,6–10,14–16,20,30–34,36,51–58]. Each of these 13 regions is densely connected with multiple other recorded regions and expresses abundant Esr1, with the exceptions of AHN, LSv, and PAG, where Esr1 expression is modest. To target Esr1-expressing cells, we injected Cre-dependent GCaMP6f viruses into each candidate region in Esr1-Cre male mice (Figures S2, S3)[6]. During the same surgery, two custom 100-μm optic fiber arrays were implanted, one targeting seven medially located regions and the other targeting five laterally positioned regions (Figures 1B, S1). A single fiber targeting lPAG was also implanted (Figure 1B). The recording setup is a modified version of previously reported setups[47,50]. It uses a low-cost CCD camera to capture images from the end of a 19-channel fiber bundle (only 13 channels

were used here) that delivers and collects, respectively, the excitation and emission light from each recording site (Figures 1C–1E).

Recordings started three weeks after the surgery, each comprised of a male, a female, and sometimes an object session (Figure 1F). The order of male and female sessions was counter-balanced. During the male session, a group-housed non-aggressive Balb/C male was introduced into the home cage of the recording male for approximately 10 minutes, while a receptive female was introduced during the female session. Figure S4 summarizes the sexual and aggressive behaviors of all recorded male mice. We observed peak fluorescence change (ΔF/F) over 100%, comparable to the Esr1 cell responses recorded using a conventional single-fiber photometry setup[5,16,20,31,33,55,59] (Figure 1G). We performed the recording two to four times for each animal, with 3–7 days between sessions. Histology was acquired for all animals. Only correctly targeted brain regions were used for a given animal. The final dataset contains 64 recording sessions from 25 animals (mean ± STD = 2.6 ± 1.0 sessions/animal), with 10.6 ± 2.2 (mean ± STD) recording sites/animal.

Large activity increase across the expanded SBN during the initial encounter with a conspecific

Upon entry of an intruder, regardless of sex, many brain regions showed remarkable Ca^{2+} activity increases (Figures 2A–2F). During the male introduction, VMHvl increased the most among all recorded regions, followed by DMH and PMv (Figures 2A, 2E, 2G, 2H). Upon female introduction, MPN showed the largest increase, with VMHvl, DMH, PMv, MeAa, BNSTpm, MeApd, and PA all showing a similarly large increase (Figures 2I, 2J). Outside the hypothalamus and amygdala, SUBv and LSv increased activity moderately, whereas the lPAG only increased activity slightly during male introduction (Figure 2G–2J). When comparing the introduction response towards males and females, VMHvl, DMH, and PMv showed a preferential response towards males, whereas MPN, BNSTpm, MeAa, and PA showed the opposite response bias, suggesting their potentially preferential involvement in male- or female-directed social behaviors (Figure 2S).

The temporal dynamics of the responses differed across regions but, interestingly, were similar during male and female entries (Figures 2K–2R). Generally, hypothalamic regions increased activity more rapidly during intruder introduction than extra-hypothalamic regions (Figures 2K–2N). During both male and female introduction, DMH rose with the shortest latency (< 1s), significantly faster than most other regions (Figures 2K–2N). PMv responded the slowest among all hypothalamic regions, with a median latency of approximately 3 s (Figures 2K–2N). Amygdala areas generally responded slower to the intruder than hypothalamic areas. MeAa and PA increased activity in 2–3 s, while MeApd took around 4 s (Figures 2K–2N). CoApm responded the slowest, with a median latency of over 6 s (Figures 2K, 2M).

The activity increases of hypothalamic regions also peaked more rapidly, with average latencies of approximately 5 s, while the responses of amygdala regions took 7–23 s to peak (Figures 2O–2R). Among the extra-hypothalamic regions, MeAa consistently demonstrated the shortest peak time, faster than MeApd and CoApm (Figures 2P and 2R). Notably, the onset latency or time to peak did not differ between male and female

intruder introduction, suggesting that, unlike the response magnitude, the temporal dynamics of a region's response are largely independent of the intruder sex (Figures 2T, 2U). Given the faster and larger hypothalamic responses than amygdala responses, it is unlikely that the hypothalamic responses result from amygdala inputs, at least initially, despite that all recorded amygdala regions, except CoApm, project directly and densely to the recorded hypothalamic regions[37,60,61]

Upon introducing a novel object, AHN, VMHvl, and DMH increased activity slightly but significantly, suggesting their activities could also be influenced by arousal or novelty (Figures S5A and S5B). However, object introduction evoked significantly lower responses than conspecific introduction (Figures S5C-S5E).

The magnitude but not the sequence of responses differs between male and female investigation

After the initial large Ca^{2+} increase upon intruder introduction, Esr1 cells in all hypothalamic and amygdala regions, except AHN, increased activity during social investigation (Figures 3A–3K, S5). During the male investigation, VMHvl showed the largest activity increase, followed by PMv, DMH, and MeApd (Figures 3C–3H). During female investigation, MPN, PA, and MeAa showed the greatest activity increase, followed by MeApd, BNSTpm, VMHvl, and PMv (Figures 3I–3J). Outside the hypothalamus and amygdala, SUBv showed a slight increase in activity, while lPAG and LSv showed no activity change during either male or female investigation (Figures 3G, 3I). We calculated the difference in Z-scored responses during male and female investigation for each recording session and found that VMHvl, DMH, and PMv ($p = 0.06$) showed male-biased responses, whereas MPN, PA, and MeAa showed female-biased responses (Figure 3K). Although investigating males and females evoked activity increase in the same ten regions, there was no significant correlation between the response magnitude to males and females across regions, suggesting distinct network activation patterns evoked by cues of each sex (Figure 3L). No region changed activity significantly during object investigation, suggesting the response is social-specific (Figures S5F, 5SG).

The temporal response patterns during male and female investigation differed across regions but were largely sex-independent (Figures 3M–3S). We compared the response onsets of two simultaneously recorded regions during trials when both regions responded significantly ($Z>2$) (Figures 3M–3S). Unlike the response during intruder entry, MeAa, instead of DMH, was the fastest to respond during both male and female investigations (Figures 3M–3S). In fact, MeAa was the only region rising before the onset of close investigation, suggesting that its activity change requires no direct contact (Figures 3N, 3Q). MeAa responded significantly earlier than MPN ($p=0.08$ for male investigation), VMHvl, and PMv, making it a possible driving force for hypothalamic activation (Figures 3O, 3R). During both male and female investigations, PMv was one of the slowest responding regions, although its activity increase was among the highest, especially during male investigation (Figures 3G, 3N, 3O, 3Q, 3R). Indeed, the fastest responsive region, MeAa, showed only a modest increase in activity during investigating males, suggesting that the response onset and magnitude are largely independent variables (Figure 3G). When comparing the response onset during male

and female investigations, only MeApd responded slightly faster during male investigation (Figure 3S). Thus, the temporal sequence of the responses during social investigation in the expanded SBN is largely invariant to the intruder's sex and is likely a stable network property.

Distinct response patterns during attack and sexual behaviors

After a period of investigation, animals expressed distinct actions towards male and female intruders. Specifically, they attacked males and mounted females. Mount refers to the process in which a male grasps a female's flank with its front paws and establishes an on-top position. Although both attack and mount involve quick movements, the network activation patterns are distinct (Figures 4, S6). During attack, the activity increase is widespread, with LSv as the only exception, consistent with its role in suppressing aggression[51,52](Figures 4A, 4C). VMHvl, DMH, and lPAG were the most activated regions, while the remaining responsive regions showed a similarly moderate activity increase (Figures 4A, 4C, 4D). Notably, lPAG and AHN only increased activity during attack, not investigation, suggesting their action-specific responses (Figures 3G, 4C). In comparison, the activity increase during mounting was more limited and graded. MPN and MeAa increased activity the most, followed by DMH, PA, BNSTpm, VMHvl, and AHN (Figures 4E, 4F). The remaining six regions did not respond (Figures 4E, 4F). The activity change during attack and mounting was not significantly correlated, suggesting a behavior-specific activation pattern (Figure 4K).

The temporal dynamics of the responses during attack and mount were also distinct (Figures 4L–4Q). During attack, VMHvl responded the fastest, increasing activity significantly earlier than MeAa, PA, PMv, and lPAG (Figures 4L–4N). lPAG was the only region that increased activity after the onset of attack, consistent with its role in driving biting during attack (Figure 4M)[55]. However, overall, there was relatively little temporal difference in the response onset among the 12 activated regions, suggesting that attack initiation may involve simultaneous activation of many regions in the limbic system (Figure 4N).

The activity increases in the hypothalamus and amygdala often preceded the mount onset, possibly because mount often follows close interaction with the female (Figures 4O–4P). Across regions, MeAa responded with the shortest latency, significantly earlier than MPN and PA, while MPN and PA increased activity earlier than BNSTpm (Figures 4P–4Q). Thus, mount involves sequential recruitment of regions in the expanded SBN.

After the male establishes an on-top position, it rapidly (22–25 Hz) and shallowly thrusts with its pelvis[62]. If the male detects the female's vagina, mount advances to deep thrust, which enables the male to insert its penis into the female's vagina[62]. After multiple deep thrusts, typically 5–20 times, the male ejaculates, characterized by ceased movement and a slow dismount[63]. As male sexual behavior advanced, the activities of different regions diverged (Figures 4G–4J, S6). MPN, BNSTpm, and PA gradually increased activity from shallow thrust to ejaculation (Figures 4G–4J, S6). The activity increase in BNSTpm during ejaculation was particularly striking, reaching a peak value 3–4 times higher than during any other period (Figures 4I, S6). In contrast, most other regions gradually decreased activity as sexual behavior progressed (Figures 4G–4J, S6). During deep thrust, there was

a widespread suppression of activity in the expanded SBN except for MPN, BNSTpm, and PA (Figures 4H–4J, S6). During ejaculation, some suppressed regions, including VMHvl, MeAa and CoApm, and lPAG, slightly increased activity, while others, such as SUBv, AHN, and DMH, were further suppressed (Figures 4J, S6). Lastly, we did not find the order of intruder presentation affect the neural responses during aggression and sexual behaviors significantly (Figure S7). Altogether, these results revealed distinct activation patterns during male aggression and sexual behaviors: the former is characterized by a widespread and simultaneous activation across many regions, while the latter features robust activation of a small set of regions and a gradual suppression of many others.

Delineation of the aggression-biased network and the mating-biased network

We then performed the principal component analysis (PCA) based on the mean Z-scored responses of all regions during various phases of social behaviors (Figure 5A). The variance in responses across behaviors could be explained nearly fully (99%) by the first four principal components (PCs) (Figure 5B). PC1 comprises responses during male sexual behaviors, especially ejaculation and deep thrust. MPN and BNSTpm have the highest PC1 score, followed by PA and MeAa, while all other regions have negative PC1 scores, consistent with their suppressed activity during late copulation (Figures 5C, 5D). PC2 is dominated by responses during male-directed behaviors, especially male investigation, and VMHvl is the region with the highest score, followed by DMH, PMv, and MeApd (Figures 5C, 5D). PC3 is again composed of female-directed behavior, but unlike PC1, mount, and shallow thrust have the highest loadings, while ejaculation has a negative loading (Figure 5C). MeAa and MPN have the highest PC3 scores, followed by PA, consistent with their activity increase during mount (Figure 5D). Finally, PC4 features a high loading during attack and negative loadings during investigation (Figure 5C). lPAG shows the highest PC4 score, followed by DMH, VMHvl, and AHN (Figure 5D).

Based on this analysis, we propose an aggression-biased network (ABN) and a mating-biased network (MBN) (Figure 5H). ABN contains six brain regions, including VMHvl, PMv, MeApd, DMH, AHN, and lPAG. AHN and lPAG are preferentially activated during attack and thus represent the motor output nodes of ABN. MBN contains four regions, including MPN, BNSTpm, PA, and MeAa. MeAa is mainly activated during mounting, BNSTpm during ejaculation, while MPN and PA are activated throughout sexual behaviors.

To further understand the distinctiveness of the activation pattern during each behavior and the ability to predict social behaviors using neural activity, we trained a discriminant analysis model for each recording session using 80% of randomly selected data points (training set). Then we predicted the behavior categories of the remaining 20% of data points (testing set). When the model was trained and tested using only frames that were annotated with a specific behavior (16% of total frames across all videos), it successfully separated the behaviors based on the neural activation patterns and predicted most behaviors accurately (F1 score (mean across behaviors ± STD) = 0.81 ± 0.11) (Figure S8). Mount and shallow thrust had relatively low F1 scores as they were sometimes misclassified as each other, possibly due to their close temporal proximity and the difficulty for humans to determine the precise transition point (Figures S8B, S8C). The F1 scores of

all behaviors were significantly higher than those predicted using time-shift models, which were constructed using MFP recording traces shifted by a random amount of time within the range of the recording session (Figure S8C).

We next trained and tested the model using all frames, including frames without specific social behaviors (annotated as “other”) (Figures 5E–5G). These “other” frames mainly involved two animals being far apart but also contained instances when animals were close but showed no discrete actions. After including these unspecified frames, we found that F1 scores (mean ± STD = 0.49 ± 0.22) decreased for all social behavior categories. The decrease in F1 score was mainly driven by misclassifying “other” frames as ones with specific behaviors and *vice versa* (Figure 5E). Interestingly, the drop in the F1 score varied widely across behaviors. For deep thrust and ejaculation, F1 scores only dropped slightly (<15%), while the F1 score for mount dropped by nearly 70% (Figures 5F, S8C). This result suggests that neural activation patterns associated with deep thrust and ejaculation are highly distinct and rarely occur outside of these behaviors during social interaction. In contrast, the activity pattern associated with mount is much less so, possibly reflecting many intended mounts that are not manifested behaviorally. Importantly, the all-frame models still predicted the behaviors significantly better than the time-shifted models for all social behavior categories (Figure 5F).

We then investigated the contribution of ABN and MBN activity in predicting the behaviors by training models using only data from non-MBN regions or non-ABN regions. When using the non-MBN model, F1 scores for all female-directed behaviors, but not male-directed behaviors, dropped dramatically compared to the full model, supporting a key role of MBN activity in determining female-directed behaviors (Figures 5F, 5G). When using the non-ABN model, F1 scores for male-directed behaviors dropped the most but notably also decreased for mount and shallow thrust, suggesting that mount initiating could require both MBN and ABN activation (Figures 5F, 5G). Notably, the activity of non-MBN and non-ABN regions could still predict male- and female-directed behaviors better than time-shifted models, suggesting that although ABN and MBN are preferentially involved in aggression and mating, respectively, they are not exclusive for the behavior (Figure 5F).

Changes in the functional connectivity during social behaviors

To address whether the functional connectivity among regions in the expanded SBN changes with social behaviors, we calculated the coefficient of determination (R^2) using 1-s moving windows (25 data points) between each pair of simultaneously recorded regions (Figure 6A). The time window was chosen based on the typical duration of a behavior episode (approximately 1–15 s, see Figure S4). Varying time windows from 0.4 to 2 s did not change the result qualitatively. To remove the auto-correlation between adjacent data points, we pre-processed the data by calculating the 1^{st} order derivative of each recording trace as the difference between adjacent data points (Figure S9). Figure 6 shows the correlation between PMv and VMHvl as an example. For the representative recording session, PMv-VMHvl had R^2 of approximately 0.09 before intruder introduction (Figures 6B, 6D). With a male intruder, R^2 jumped to 0.15, further increased to 0.25 during male investigation, and peaked at 0.44 during attack (Figures 6B–6D). PMv-VMHvl correlation also increased in the

presence of a female intruder and was further elevated during female investigation (Figure 6D). However, the correlation gradually decreased as the sexual behaviors advanced and reached a level below the pre-intruder baseline during deep thrust and ejaculation (Figures 6C, 6D). These functionality connectivity changes were consistent across recording sessions from different animals (Figures 6E–6M).

One crucial question is whether the correlation change during social behavior simply reflects changes in motor output. We thus calculated R^2 for all pairs during the low (bottom 25%) and high-velocity (top 25%) periods when the animal was alone in the cage. Although no pair of regions showed a significant change in R^2 with velocity, we noticed that connections involving lPAG, SUBv, BNSTpm, PA, and LSv tended to increase strength during the high-velocity period (Figures S10A-S10C). To further address the question, we identified the time points when the locomotion initiated (reach peak speed >8 pixel/fr) after a quiescence period (mean speed < 1 pixel/fr for > 1s) and constructed PSTHs of R^2 aligned to the movement onset (Figures S10D, S10E). This analysis confirmed functional connectivity between regions involving lPAG, SUBv, BNSTpm, PA, and LSv increased after movement initiation. However, functional connections among hypothalamic regions, medial amygdala, and cortical amygdala were largely invariant to the movement (Figures S10F, S10G). Thus, although movement may contribute to changes in functional connectivity between some regions, it minimally modulates the connectivity among the hypothalamus, medial and cortical amygdala.

We then examined the functional connectivity across all 78 pairs of regions during different social behaviors and reached several general conclusions. First, some regions showed a significant correlation in activity even at the baseline (Figures 7A, 7B). This baseline correlation may be considered the resting-state connectivity. The strongest functional connectivity was observed among amygdala regions, including MeApd, PA, CoApm, and SUBv, or connections involving lPAG (Figures 7A, 7B). After intruder introduction but in the absence of social interaction, the functional connectivity pattern remained unchanged except for strengthening the VMHvl and PMv connection, especially with the male intruder (Figures 7A, 7C, 7F). During male investigation, the correlation among VMHvl, PMv, and DMH increased significantly (Figures 7A, 7D). During female investigation, there was a broad weak increase in functional connectivity (Figures 7A, 7G). The most striking changes in correlation occurred during the social behavior initiation phase. During attack, the functional connectivity between 95% of pairs in the social network increased significantly (Figures 7A, 7E, 7L-7N). Intriguingly, the increase in functional connectivity does not require a net change in Ca^{2+} activity. For example, although LSv did not show an increase in response during attack, its functional connectivity with the rest of the expanded SBN nevertheless increased (Figures 7A, 7L). During mounting, there was also an overall increase in connectivity in the expanded SBN, but interestingly not for connections involving the VMHvl (Figures 7A, 7H, 7L-7N). As the sexual behavior advanced, we observed a general decorrelation in the network (Figures 7A, 7I-7N). During shallow thrust, the connectivity largely returned to the baseline level except for several weakly strengthened connections involving BNSTpm, MPN, PA, lPAG, and AHN (Figures 7A, 7I, 7L). During deep thrust and ejaculation, most connections weakened, some reaching a level significantly below the pre-intruder baseline (Figures 7A, 7I-7N). Interestingly, during this “dissociated”

network state, the male showed a drastic decrease in response to external sensory cues. While a brief air puff (1s, 12 pSi) consistently disrupted males' ongoing behavior before female introduction or after ejaculation, the male was impervious to the air puff during deep thrust and continued to thrust (Figure S11). The dissociated state during thrust and ejaculation was short-lived. The network connectivity largely retuned to the pre-female state after female removal, regardless of whether ejaculation occurred or not (Figure S12).

Introducing a small jitter (40–200 ms) into the simultaneously recorded Ca^{2+} traces abolished the across-region correlation during all behaviors, suggesting that the correlation is highly sensitive to the precise alignment of activities between regions (Figure S13). Altogether, these results suggest that initiating social actions involve coordinated activation across the social network, including regions that appear to show no net change in activity. Intriguingly, advanced sexual behaviors are accompanied by a "dissociated" brain state.

DISCUSSION

Using a modified multi-site optical recording system, we examined the neural activities across multiple regions in the limbic system during sexual and aggressive behaviors in male mice. These recordings revealed widespread activities in the network that evolved in distinct ways throughout male-male and male-female social interactions.

The overall activation pattern in the expanded SBN during male social behaviors

We characterized three aspects of the Ca^{2+} responses during social behaviors: magnitude, timing, and functional connectivity among regions (Figure S14). Overall, the response magnitude is behavior- and intruder sex-specific, whereas the timing is behavior- but not intruder sex-specific. Network connectivity increases drastically during the fast action phase of social behaviors and decreases during late copulation.

Most recorded regions showed the maximum activity increase during the initial intruder encounter. This is perhaps not surprising as the net change of sensory cues was the largest at that moment. The entry response was generally higher and faster in the hypothalamus than amygdala, possibly reflecting a higher level of information convergence and a lower spontaneous activity in the hypothalamus. DMH was consistently the first (<1s) to respond regardless of the intruder sex, and this response occurred before the physical interaction of the two animals (median latency of first interaction: 3.7 s for male intruders and 3.6 s for female intruders), suggesting its potential role in the initial detection of distant social targets. Several regions in the ABN, including VMHvl, DMH, and PMv, showed higher responses to males than females, while all MBN regions, including MeAa, PA, BNSTpm, and MPN, showed the opposite preference. Thus, information regarding the intruder's sex is represented widely in the expanded SBN quickly after intruder introduction.

Ten out of thirteen regions were activated significantly during social investigation, all responding to both males and females. The response magnitude in most regions showed sex biases. Interestingly, MeAa, instead of DMH, was the first to increase activity during each episode of social investigation, and it was also the only region to respond before the investigation onset. Like MeApd, MeAa receives extensive inputs from the accessory

olfactory bulb and projects densely to the medial hypothalamus and other olfactory-related amygdala regions[64]. However, it has received less attention as immediate early gene studies found that handling, tail pinch, mating, and fighting all activate the MEAa, leading to the conclusion that MeAa belongs to a general arousal circuit[1,65,66]. Here, we found MeAa^{Esr1} cells respond rapidly and specifically during female but not object investigation, suggesting its potential social-specific role. Interestingly, compared to MeApd, MeAa projects more densely to the ventral striatum and ventral tegmental area, regions essential for social interest[45,64,67].

The activity changes during attack and mount differed vastly. Attack was accompanied by activity increases in all regions except the LSv, an aggression "gating" region[52]. VMHvl demonstrated the fastest and largest response during attack, preceding several other aggression-related regions, including PA, PMv, and PAG, suggesting VMHvl as the attack "ignitor"[30–34,55]. However, VMHvl does not mediate attacks on its own. The functional connectivity of nearly the entire expanded SBN strengthened drastically during attack. Thus, although the attack signal may originate from the VMHvl, its continuation likely requires the entire network. Thus, modulating many nodes in the network could cause changes in attack[9,10,30,31,33,34,36,51,52,54,55].

Mount was accompanied by a relatively limited network activation. It involved seven activated regions vs. twelve during attack. MPN and MeAa demonstrated the highest responses. Interestingly, the activity rise in the MeAa was earlier than MPN, the most-established region for male sexual behavior. While MeAa activity increase may partially reflect changes related to social investigation, which often precedes mounting, we did not find MeAa as the first to respond during attack, which also frequently follows close interaction. At the network level, the functional connectivity between many regions increased during mounting as in the case of attack, but connections involving VMHvl remained largely unchanged. This perhaps explains the weak deficits in mounting when VMHvl is artificially inhibited, even though VMHvl is one of the regions with increased activity during mounting[3,6–8]. As sexual behavior advanced, we saw a clear divergence of activity patterns across regions. PA, MPN, and BNSTpm were the only regions that gradually increased activities, peaking during ejaculation, while all other regions gradually decreased activities. The neural activity pattern during late sexual behavior was highly distinct and could be used to predict the behaviors reliably. During late sexual behaviors, the most striking change at the network level was an overall decrease in functional connectivity. No connection was strengthened, regardless of whether it was between regions responsive or not, and many dropped below the baseline level. This result suggests the brain enters a "dissociated" state during late mating. Interestingly, male rats are reported to have drastically reduced sensitivity to pain during copulation[68,69]. We further demonstrated that male mice are oblivious to the air puff during deep thrust. Whether these behavior changes result from decreased communication across brain regions remains to be investigated.

Although we focused on Esr1 cell responses during mating and fighting, these cells are also relevant for other social behaviors, such as parental care and infanticide[16,70,71]. We chose Esr1 cells as we aim to target various regions in the social network, making it challenging to use markers specific to one region or one behavior. However, it is almost certain that some

Esr1 cells in each recorded region are irrelevant to the behavior of focus. Indeed, several recent single nucleus RNA sequencing (snRNAseq) studies revealed molecularly distinct clusters within the Esr1 population[19,72]. Future studies should refine the molecular identity of cells in each region of the MBN and ABN. Additionally, we could not rule out the possibility that some non-Esr1 cells are also important for mating and fighting. For example, half of the PA cells projecting to the VMHvl do not express Esr1, although their functional role remains unknown[31]. Nevertheless, several studies comparing Esr1 positive and negative cells in the same region concluded that the Esr1 positive cells are preferentially activated during social behaviors[6,70,73].

The mating-biased network

We propose that MPN, BNSTpm, PA, and MEAa form the MBN to support male sexual behaviors. These regions, except MeAa, showed a consistent increase during all stages of male sexual behaviors, with higher responses in more late stages. The activity increases probably reflect a combination of sensory inputs (e.g., olfactory and somatosensory) and internal cues (e.g., hormone and neuromodulator) and may be used to drive moment-to-moment actions associated with mating.

MPN is unarguably the most studied region for male sexual behaviors. Since 1941, numerous studies have demonstrated that MPN damage impairs or abolishes male sexual behaviors without spontaneous recovery, suggesting its irreplaceable role in mating[74]. Both c-Fos and *in vivo* recordings corroborate functional results[16]. Our recordings further confirm the large increase in MPN activity throughout the male sexual behaviors. However, we do notice some heterogeneity in MPN responses across animals. In animals with optic fibers located in posterior MPN, the cell responses to females tended to be weaker than those with anterior MPN-targeted fibers (although all animals were included in the analysis). Our recent study suggests that posterior MPN is mainly activated when facing social threats and plays a vital role in suppressing aggression against superior opponents[75].

The role of BNSTpm in male sexual behaviors has been long suspected based on its remarkably dense c-Fos expression after male mating[66,76–78]. Recent functional studies reported significantly impaired male sexual behaviors after ablating or inhibiting BNSTpm aromatase, Tac1, or Esr1 expressing cells[19–21]. Additionally, Zhou et al. reported that BNST Esr2-expressing cells, a subset of Esr1 cells, are important for ejaculation-induced sexual refraction[19,22]. These findings corroborate our observations that BNSTpr^{Esr1} cells are activated during various stages of male sexual behaviors, with a particularly striking activity increase during ejaculation.

PA has largely escaped the attention of neuroscientists, possibly due to its relatively low c-Fos induction after sexual behaviors[79]. Nevertheless, our recent functional studies demonstrated that PA^{Esr1} cells are necessary and sufficient for male sexual behaviors through their projection to the MPN[31]. Most strikingly, when the PA^{Esr1} to MPN projecting cells are inhibited, males rarely mount and never achieve deep thrust[31].

The role of MeAa in sexual behaviors remains elusive. Early studies found that MeAa lesions could abolish all aspects of male sexual behaviors[80]. However, the MeApd, but

not MeAa, expressed c-Fos specifically after exposure to female pheromone cues and consequently became the focus of many studies[81]. However, recent cell type-specific ablation argued against the important role of MeApd in male sexual behaviors[10]. Consistent with these functional results, we found no significant activity increase of MeApd^{Esr1} cells during male mating. Given the intense and rapid activation of MeAa during the early phase of male sexual behavior, future studies are needed to investigate its function in male sexual behaviors.

The aggression-biased network

The proposed ABN contains AHN, DMH, VMHvl, PMv, MeApd, and lPAG based on their preferential responses during aggression over sexual behaviors. Here, we will summarize their known functional roles in aggression and highlight the new insights revealed by our recordings. Notably, although PA, BNSTpm, and MPN show preferential responses during male sexual behaviors, they also play a role in male aggression.

VMHvl has now been firmly established as a critical site for conspecific aggression [6–8]. Consistent with its critical role in aggression, VMHvl shows the largest response during male introduction, investigation, and attack. VMHvl is the first to respond and one of the top regions to increase functional connectivity during attack, supporting its central role in attack initiation.

PMv is a major input to the VMHvl and is highly responsive to conspecific olfactory cues[33,82]. Indeed, PMv is among the most activated regions during male investigation. However, PMv response during attack is relatively weak and significantly slower than the VMHvl, suggesting its secondary role in initiating attack. It also suggests that the rise of VMHvl activity during attack is unlikely a result of olfactory inputs channeling through the PMv.

DMH has only been studied recently for its role in aggression. Zelikowsky et al. found tachykinin-expressing DMH cells necessary and sufficient for social isolation-induced aggression in male mice, although the cell response during attack was not reported[54]. We found that DMH, like VMHvl, showed a male-biased response during all stages of social behaviors. Whether DMH influences aggression through its connection with VMHvl or its parallel projection to PAG remains to be investigated.

Recent studies demonstrated a necessary and sufficient role of MeApd GABAergic cells in inter-male aggression[9–13], although the cell Ca^{2+} responses during attack remain unreported. Consistent with the functional results, we found that MeApd^{Esr1} cells increased their activity during both attack and male investigation. MeApd also substantially increased its functional connectivity during attack, especially with VMHvl, supporting its important role in attack initiation.

lPAG^{Esr1} cells showed increased activity exclusively during attack, consistent with classical lesion and electric stimulation studies showing PAG's ability to modulate attack bi-directionally in rats[83,84]. We previously found lPAG as a key downstream of VMHvl for attack initiation, although stimulating the VMHvl-lPAG pathway only induces attacks with

low efficiency[55]. Indeed, most ABN regions project to lPAG[85], which may be a common gateway to integrating ABN inputs to initiate action. Thus, blocking lPAG is sufficient to block attack, whereas activating any specific input only triggers attack weakly or not at all[55].

AHN was considered a part of the aggression circuit based on early studies in hamsters[86,87]. However, later, AHN was proposed as a part of the predator defense circuit given its strong c-Fos activation after predator encounters[88,89]. Recently, Xie et al. reported that AHN GABAergic cells (the main population) bi-directionally control defensive attacks against both predators (e.g., snakes) and aggressive conspecifics in mice[53]. We found that AHN^{Esr1} cells uniquely increased activity during the action phase of aggression. Thus, AHN may promote attack but is not socially specific.

Although PA is included in the MBN, PA also plays a role in male aggression through its projection to VMHvl[30–32]. PA is consistently activated during male investigation and attack, although the responses during female investigation and sexual behaviors are significantly higher. The female-biased response could partly reflect our sampling bias. We likely mainly record from PA-MPN cells given that they are more dorsally located than PA-VMHvl cells, and our optic fiber was placed above the PA dorsal surface[31]. Our previous study showed higher responses of PA-VMHvl cells during male-male than male-female interaction[31].

Similar to PA, BNSTpm could modulate aggression despite being a part of the MBN. However, its exact role in aggression remains elusive. On the one hand, inhibiting BNSTpm Esr1, aromatase, or Tac1 and Esr1 co-expressing cells all reduced attack in male mice, supporting a positive role of BNSTpm in aggression[19–21]. On the other hand, no study reported acutely increased aggression after BNSTpm activation[19–21]. In fact, activating BNSTpm aromatase cells suppressed aggression[20]. Consistent with a negative role of BNSTpm in aggression, optogenetic stimulation of the projection from MeA to BNSTpm, which is primarily GABAergic and presumably inhibits BNSTpm cells, promoted aggression[12]. In our study, although BNSTpm^{Esr1} cells are significantly activated during attack, they are among the slowest responding cells, suggesting they likely do not play a key role in initiating attack.

LSv is the only region showing no activity increase during attack. It is also the only region whose connection with VMHvl does not strengthen during attack. LS has been recognized as an aggression “gating” region for decades. Early studies demonstrated “septal rage”, i.e., unprovoked ferocious attack[90], caused by the septal lesion. Recent studies confirmed that LS could suppress aggression through its GABAergic projection to VMHvl[51,52]. Given these functional results, the lack of activity increase in LSv may signal “permission” to attack.

In summary, we investigated Ca^{2+} responses in the expanded SBN during social behaviors in male mice. Our results suggest that sex identity information is broadly represented across the network. Fighting and mating are associated with distinct network activation patterns. Attack features synchronized activation of many regions, with VMHvl being the potential ignitor. Sexual behavior is associated with the sequential activation of a small set of regions and their gradual changes during behavior progression. The network activity during late copulation is particularly unique, featuring strong activation of three regions, suppression

of others, and reduced communication across regions. These results provide a holistic view regarding the neural generation of social behaviors and will serve as an important guide for future functional studies, which are likely to refine and revise the identity and composition of the MBN and ABN.

STAR★METHODS

RESOURCE AVAILABILITY

Lead contact—Further information and requests for resources and reagents should be directed to and will be fulfilled by the lead contact, Dayu Lin (dayu.lin@nyulangone.org).

Materials availability—This study did not generate new unique reagents.

Data and code availability

- The relevant multi-fiber photometry recording dataset has been deposited at Zenodo and is publicly available as of the date of publication. The accession number is listed in the key resources table.
- All Matlab codes generated in this manuscript have been deposited at Zenodo and are publicly available as of the date of publication. The accession number is listed in the key resources table.
- Any additional information required to reanalyze the data reported in this paper is available from the lead contact upon request.

EXPERIMENTAL MODEL AND SUBJECT DETAILS

Mice—Experimental mice for MFP recording were socially naïve, Esr1-Cre male mice (10–24 weeks, Jackson stock no. 017911). After surgery, all test animals were single-housed. Intruders used were group-housed BALB/c males or group-housed C57BL/6 females (both 10–36 weeks, Charles River). Mice were housed at 18–23 °C with 40–60% humidity and maintained on a reversed 12-h light/dark cycle (dark cycle starts at 10 a.m.) with food and water available ad libitum. All experiments were performed in the dark cycle of the animals. All procedures were approved by the IACUC of NYULMC in compliance with the NIH guidelines for the care and use of laboratory animals.

METHOD DETAILS

MFP recording setup—The optical setup was a modified version of a typical fiber photometry setup according to a previously described multi-fiber photometry recording systems[47,50]. Briefly, blue LED light (Thorlabs, M470F1, LEDD1B) was bandpass filtered (Semrock, FF02–472/30–25), reflected on a dichroic filter (Semrock, FF495-Di03–25×36), and coupled into a custom-designed 19-fiber multi-fiber bundle (Doric Lenses, BFP(19)_100_110_1100–0.37_4m_FCM-19X) through a 10x objective (Olympus PLN). Emission light was bandpass filtered (Semrock, FF01–535/50) and projected onto the CCD sensor of a camera (Basler, acA640–120um) via an achromatic doublet (Thorlabs, AC254–060-A-ML). The connector end of the fiber bundle was imaged by the camera. The LED was

driven by DC current, and the optical power out of the tip of every single fiber was set to be ~30 μW. The sampling rate of the camera was 25 frames per second.

Stereotaxic surgery—Esr1-Cre mice were anesthetized with 1.5%–2% isoflurane and placed on a stereotaxic surgery platform (Kopf Instruments, Model 1900). 60–100 nl AAV2-CAG-FLEX-GCaMP6f (Vigene, custom prepared) or AAV1-CAG-FLEX-GCaMP6f (Addgene, 100835-AAV1, 3x dilution) was delivered unilaterally into each of the following targeted brain regions: LSv (AP 0.05, ML −0.65, DV −3.25); MPN (AP 0.00, ML −0.33, DV −4.90); BNSTpm (AP −0.30, ML −0.80, DV −3.60); AHN (AP −1.05, ML −0.55, DV −5.15); DMH (AP −1.75, ML −0.55, DV −5.2); VMHvl (AP −1.70, ML −0.75, DV −5.80); PMv (AP −2.40, ML −0.55, DV −5.70); MeAa (AP −1.10, ML 2.10, DV −4.90); MeApd (AP −1.60, ML 2.10, DV −4.92); PA (AP −2.35, ML 2.20, DV −4.92); CoApm (AP −2.85, ML 2.90, DV −5.20); SUBv (AP −3.35, ML 2.60, DV −4.60); lPAG (AP −4.90, ML −0.45, DV −2.40). All regions included in the final analyses had correct virus expression and fiber tip position based on histology.

The multi-fiber arrays were constructed using MT Ferrules (US Conec, No 12599) and 100 μm-core optic fibers (Doric Lens, NA0.37) as described previously[50]. The connector contains 4 × 12 through holes, spaced by 250 μm (center-to-center distance). Each hole can fit one 100-μm optic fiber. The positions of the holes were selected based on the anatomical relationship of the brain regions of interest. The length of each optic fiber was determined based on the depth of the targeted region. Once all fibers were inserted into the correct positions below the ventral surface of the connector, they were secured with super glue. The other end of the fibers was then cut and polished. For each animal, two custom-made multi-fiber arrays were implanted, one designed to target seven medial regions on the left hemisphere and the other to target five lateral regions on the right hemisphere. Figure S1 shows the locations of all the fibers within the connectors for targeting medial and lateral structures. A custom-made optic-fiber assembly targeting lPAG (Thorlabs, CFX126–10) was also implanted in the same animal. All optic fibers are targeted ~250 μm above the injection sites and secured using dental cement (C&B Metab ond, S380). lPAG fiber was implanted at (AP −5.20, ML −0.45, DV −2.00) after tilting the head 8 degrees down rostrally to avoid collision with the other two arrays. Lastly, a 3D-printed plastic ring for head fixation was cemented on the skull[93].

Behavioral analysis and tracking—Behaviors were recorded under dim room light via two cameras from top and side views (Basler, acA640–100gm) using StreamPix 5 (Norpix), which also coordinated the MFP camera in synchrony. Behaviors were then manually annotated, and animal positions were tracked on a frame-by-frame basis using custom software in MATLAB (https://pdollar.github.io/toolbox/). Annotated behaviors are defined as follows: ‘Investigation’, the resident mouse made nose contact with either the facial or anogenital region of the intruder mouse or the whole body of the toy mouse; ‘Attack’: a suite of actions initiated by the resident toward the male intruder, which included lunges, bites, tumbling and fast locomotion episodes between such behaviors; ‘Mount’: began when the resident male charged toward the rear end of the female body, rose and grasped the female’s flank with his forelimb, and ended by aligning his body with the female’s and assuming

the on-top posture; ‘Shallow thrust’: the male grasped the female’s body tightly with his forelegs and made rapid shallow pelvic thrusts; ‘Deep thrust’: deep rhythmic movement of pelvis presumably with penile insertion into the vagina; ‘Ejaculation’: the male froze at the end of an intromission event while continuously clutching onto the female and then slumping to the side of the female. Ejaculation occurred only once in a female session, signaling the end of sexual behaviors. It was always confirmed by the presence of a vaginal plug after the recording. Behavioral annotations were made by trained experimenters, during which neural responses were not available to the experimenter. The animals were tracked using custom MATLAB software (https://github.com/pdollar/toolbox)[8,94]. The velocity of the animal was calculated as the distance between the animal’s body center locations in adjacent frames (pixels/s).

Multi-fiber photometry recording—The recording started three weeks after the virus injection. For each recording session, the head-mounted MT ferrules were connected to the matching connectors at the end of the optic fiber bundl e (Doric lens, BFP(19)_100/110/1100–0.37_4m_SMA-19x). A drop of liquid composite (Henry Schein, 7262597) was applied to the outer part of the junction and cured with blue LED curing light (Amazon) to stabilize the connection. The baseline signal was checked in the absence of the intruder for at least two days to ensure that the signal reached a stable level (<10% difference across days for all regions). On the recording day, after 10 minutes of the baseline period, a sexually receptive female or a group-housed non-aggressive male mouse was introduced. Ten minutes after the first intruder was removed, a second intruder of a different sex was introduced. For the female session, it ended when the recording male achieved ejaculation or after 60 minutes. If the female was clearly rejective (although all females were screened with experienced mounters briefly before the recording to ensure sexual receptivity), the session would be terminated earlier. The male session generally lasted for 10–15 minutes. The order of male and female presentations was counterbalanced across sessions. For some recording sessions, 10 minutes after removing the male, a novel object (15 mL plastic tube) was introduced for 10 minutes. Each animal was recorded 2–4 times, with at least three days in between.

Data analysis—Regions of interest (ROIs) for selected channels were drawn on the grayscale image of the optic fiber bundle, and the average pixel intensity for each ROI was calculated as a readout of the raw Ca^{2+} signal (Fr^{aw}) for the region. We then used the MATLAB function “msbackadj” with a moving window of 10% to get the flatted signal F_{flat}. Then the instantaneous baseline signal was obtained as $F_{baseline} = F_{raw} - F_{flat}$. The $\Delta F/F$ was then calculated as $\Delta F/F = (F_{raw} - F_{baseline})/F_{baseline}$. The $\Delta F/F$ signal was then Z-scored using the entire recording trace for each channel. All analyses were based on Z-scored $\Delta F/F$.

The response magnitude of each behavior for each recording animal was calculated by first averaging Z-scored $\Delta F/F$ during all episodes of the behavior in a session and then averaging the values across all recording sessions of an animal. The difference in response magnitude between two regions was calculated as the difference of average responses of two simultaneous recorded regions of a session and analyzed across all sessions. To compare

responses during male-directed and female-directed behaviors (e.g., male investigation vs. female investigation), we calculated the magnitude difference between the behavior towards the male intruder and the female intruder of each session and analyzed all sessions. To calculate the onset of the response of behavior, e.g., attack, we first selected responsive trials when the Z-scored ΔF/F reached >2. For those trials, we then determined the trough time preceding the peak response after smoothing the trace with a low pass filter (threshold 4 Hz). If a session contained at least three responsive trials (Z>2), the average onset time of the behavior of the session was computed. Otherwise, the onset would be registered as NaN. To compare the onset time during male-directed and female-directed behavior, e.g., male investigation vs. female investigation, we determined the average onset during each behavior in one session and calculated their difference. To compare the onset time of two different regions in one behavior, we identified trials where both regions showed a peak response >2, determined the response onset for each, and calculated the difference. We then performed a two-sided t-test (if data passed the normality test) or Wilcoxon signed-rank test (if data did not pass the normality test) on the onset time difference using all trials with a null hypothesis that the onset difference was 0. The peak time during introduction was determined as the latency to reach the maximum value in the first 30s after intruder introduction. The peak time difference between the two regions was calculated based on the peak time of simultaneously recorded traces. The PETHs were constructed by aligning the Z-scored ΔF/F to the onset of a behavior, averaging across trials, averaging across sessions for each animal, and then averaging across animals.

Principal Components Analysis (PCA) was performed using the MATLAB function “pca.” The data submitted to PCA was a 13 × 9 matrix (corresponding to 13 regions and 9 behaviors) whose i^{th}, j^{th} element is the response magnitude (Z scored ΔF/F) of the i^{th} region during the j^{th} behavior averaged first over trials, then sessions, and finally subjects. The first four components explained over 99% of the variance.

A linear discriminant model for each recording session was constructed using the MATLAB function “fitcdiscr “using 80% of randomly selected data (training data). The model was then used to predict the behaviors associated with the remaining 20% (testing data) of the Ca^{2+} recording data in each session using MATLAB function “predict”. We used either all the frames (Figure 5) or the frames annotated with specific social behaviors (Figure S8) for training and testing. For each session, only channels with correct targeting were used for training and testing the model. The confusion matrix was constructed based on all the testing data from all sessions of all animals. F1 score was calculated as (2 × precision × recall) / (precision + recall) for each behavior and each recording session and averaged across sessions. To calculate the F1 score of time-shifted data, the recording traces of all channels were shifted by a random offset (0 to the duration of the recording session) and used for constructing the discriminant model and predicting the behaviors. This procedure was performed once for each session.

For assessing the contribution of MBN and ABN regions to behavior prediction, we constructed the discriminant models based on recordings from non-MBN regions or non-ABN regions and used the model to predict the behaviors. We then compared the F1 scores for each behavior obtained using the full model, non-MBN model, non-ABN model, and

time-shifted model using pairwise comparisons. Generally, the full model predicted all the behaviors significantly better (higher F1 score) than all other models, and non-MBN and non-ABN models still predicted behaviors better than the time-shifted model. For Figure 5F and Figure S8C, each subject's F1 scores were computed separately by concatenating results across sessions.

To determine the instantaneous coefficient of determination (R^2) between two regions, we first calculated the first derivative of the Z-scored ΔF/F trace as the difference between adjacent data points (25 points/sec). We then computed the moving-window correlation (window size: 25 data points) using the MATLAB function "movcorr" and its elementwise squaring as R^2. We then calculated the average R^2 during each behavior for each recording session and the average of all sessions. To determine whether R^2 changed significantly during a behavior, we performed paired t-test (if data passed the normality test) or sign test (if data did not pass the normality test) between the averaged R^2 during the behavior and that during the baseline period of the same session across all sessions. The p values were adjusted using Benjamini & Hochberg procedure for controlling the false discovery rate (FDR). The graph plot for each behavior was generated using MATLAB function "graph". The averaged R^2 values during the behavior for all pairs of regions (76 in total) were used as the weights of connections and indicated as the width of the lines. Only connections with R^2 >0.1 were shown. The size of a node is proportional to the accumulated weight (R^2) of all the connections involving the node. The graph plots in Figure 7B convey similar information as the heatmap in Figure 7A (indicated as the line width of connections) and 7L (indicated as the node size). To determine the importance of the temporal alignment on the correlation between regions, we added a slight jitter (randomly selected from 40, 80, 120, 160, and 200 ms) to one of the Z-scored ΔF/F traces in each pair of regions and then calculated the R^2 of all pairs.

To determine the relationship between the movement velocity and correlation between regions, we tracked the animal and calculated its body center velocity and the average R^2 in the frames with the top 25% movement velocity and those with the bottom 25% velocity for each session. We then calculated the difference between each session's low-velocity and high-velocity periods and the average across sessions. To determine the onset of movement during the baseline period, we determined troughs and peaks in the velocity trace and selected troughs that precede peaks reaching at least 8 pixels/fr and follow >1s of quiescence (mean velocity < 1pixel/fr). We then constructed PSTHs of R^2 of each pair of regions aligned to the movement onset in each session and calculated the average for each session and the average PSTHs of all sessions. We then calculated the difference in averaged R^2 between post- (0 −1 s) and pre-movement (−1 – 0 s) based on the PSTHs. The movement-sensitive pairs (red-filled circles in Figure S9F and red trace in Figure S9G) are pairs with a ΔR^2> 0.01.

Behavior disruption by air puffs—Mice were anesthetized with 1.5% isoflurane and equipped with a 3D-printed head ring affixed to the skull using dental cement. A 0.25" piece of an 18G blunt needle (SAI, B18–50) was unilaterally cemented to the head-post exterior, pointing to the eye and whisker region of the mouse. Mice were allowed to recover (>1 week) and were then habituated to the recording chamber. Before each test

session, a long segment of tubing (Tygon tubing, 1/32” ID, 3/32” OD, lot #25370284) was carefully attached to the blunt needle while the animal was head-fixed. The mouse was immediately transferred to the home cage, where he could move freely with the flexible tubing attachment. A pressurized central building air supply wall outlet was connected to a pressure regulator (NITRA pneumatics, 1/8” NPT, AR-212), which was then connected to a standard 2-way normally closed (NC) isolation valve (NResearch, 161T011). The valve was wired to receive 12V of power and TTL pulses via a BNC cable connected to a TDT RX8 I/O system. Pulses were gated via a 12V 1-channel relay module (HiLetgo). During different behaviors, pulses were remotely and manually triggered to open the isolation valve for 1 second and release a 12 PSI (pounds per square inch) air puff. For each trial, we observed the videos frame-by-frame and manually determined whether the mouse reacted to the puff or not based on the occurrence of abrupt movement or termination of ongoing behaviors. Further, DeepLabCut (DLC) was used to track the head of the animal[92]. We then calculated the head velocity as the head displacement between two adjacent frames and constructed the velocity PETHs aligned to the air puff onset.

Histology and imaging—Mice were over-anesthetized with isoflurane and transcardially perfused with cold 1x phosphate-buffered saline (PBS), followed by cold 4% paraformaldehyde (PFA) in 1x PBS. Heads with implants were post-fixed in 4% PFA for at least 72 h at 4°C and then transferred into 15% sucrose solution for 48 h, after which brains were carefully extracted and put into 15% sucrose solution at 4°C overnight. Brains were embedded in OCT mounting medium, frozen on dry ice, and cut into 50 μm-thick sections using a cryostat (Leica). Sections were collected in a 6-well plate, washed three times with 1x PBS, and counter-stained with DAPI (1:20,000; Thermo Fisher, D1306) diluted in PBS-T (0.3% Triton X-100 in 1x PBS) for 15 min. After washing with PBS-T once, sections were mounted on Superfrost slides (Fisher Scientific, 12–550-15) and cover-slipped for imaging via a slide scanner (Olympus, VS120). 10x fluorescent images were acquired to access fiber placements and virus expressions.

QUANTIFICATION AND STATISTICAL ANALYSIS

All statistical analyses were performed using MATLAB 2021a (MathWorks) or Prism 9 (GraphPad). All datasets were tested for normality with the Lilliefors test whenever applicable. Parametric tests, including one-sample t-test, paired t-test, and ordinary one-way ANOVA and multiple-comparison post hoc tests, were used if distributions passed the normality test. If distributions failed the normality test, non-parametric tests, including one-sample Wilcoxon signed rank test, Wilcoxon signed rank test, Friedman test, and Kruskal-Wallis test, were used. P values for all multiple one-sample t-tests, one-sample Wilcoxon signed rank tests, multiple pairs of t-tests, and post-hoc multiple-comparison tests were adjusted using Benjamini & Hochberg procedure for controlling the false discovery rate. All tests are two-sided. Significance in all statistical results was indicated as follows: * $p < 0.05$, ** $p < 0.01$, and *** $p < 0.001$. Error bars were presented as mean ± s.e.m if most datasets in a figure plot passed the normality test. Otherwise, error bars were presented as median ± 25%. No statistical methods were used to predetermine sample sizes, but our sample sizes were similar to or larger than those reported previously. Statistical details and sample size can be found in the figure legends and Table S1.

Supplementary Material

Refer to Web version on PubMed Central for supplementary material.

ACKNOWLEDGEMENTS

We thank Dr. Yaroslav Sych for the advice on constructing the multi-fiber arrays and tips for achieving stable recordings. We thank Yiwen Jiang for help maintaining the mouse colony and all Lin lab members for helpful discussion and feedback on the project. This research was supported by NIH grants R01MH101377, R01MH124927, R01HD092596 and U19NS107616 (D.L.); R01MH118928 and RF1DA056394 (Z.S.C). The Mathers Foundation and the Vulnerable Brain Project (D.L.). The Leon Levy Neuroscience Fellowship and NIMH K99MH127295 (J.E.L). The Uehara Memorial Foundation and Osamu Hayaishi Memorial Scholarship (T.O.). Basic Science Research Projects from Sumitomo Foundation (T.Y).

REFERENCES

1. Newman SW (1999). The medial extended amygdala in male reproductive behavior. A node in the mammalian social behavior network. Ann N Y Acad Sci 877, 242–257. 10.1111/j.1749-6632.1999.tb09271.x. [PubMed: 10415653]
2. Goodson JL (2005). The vertebrate social behavior network: evolutionary themes and variations. Horm Behav 48, 11–22. 10.1016/j.yhbeh.2005.02.003. [PubMed: 15885690]
3. Yang T, Yang CF, Chizari MD, Maheswaranathan N, Burke KJ Jr., Borius M, Inoue S, Chiang MC, Bender KJ, Ganguli S, and Shah NM (2017). Social Control of Hypothalamus-Mediated Male Aggression. Neuron 95, 955–970 e954. 10.1016/j.neuron.2017.06.046. [PubMed: 28757304]
4. Hashikawa K, Hashikawa Y, Tremblay R, Zhang J, Feng JE, Sabol A, Piper WT, Lee H, Rudy B, and Lin D (2017). Esr1+ cells in the ventromedial hypothalamus control female aggression. Nat Neurosci. 10.1038/nn.4644.
5. Falkner AL, Grosenick L, Davidson TJ, Deisseroth K, and Lin D (2016). Hypothalamic control of male aggression-seeking behavior. Nat Neurosci 19, 596–604. 10.1038/nn.4264. [PubMed: 26950005]
6. Lee H, Kim DW, Remedios R, Anthony TE, Chang A, Madisen L, Zeng H, and Anderson DJ (2014). Scalable control of mounting and attack by Esr1+ neurons in the ventromedial hypothalamus. Nature 509, 627–632. 10.1038/nature13169. [PubMed: 24739975]
7. Yang CF, Chiang MC, Gray DC, Prabhakaran M, Alvarado M, Juntti SA, Unger EK, Wells JA, and Shah NM (2013). Sexually dimorphic neurons in the ventromedial hypothalamus govern mating in both sexes and aggression in males. Cell 153, 896–909. 10.1016/j.cell.2013.04.017. [PubMed: 23663785]
8. Lin D, Boyle MP, Dollar P, Lee H, Lein ES, Perona P, and Anderson DJ (2011). Functional identification of an aggression locus in the mouse hypothalamus. Nature 470, 221–226. 10.1038/nature09736. [PubMed: 21307935]
9. Hong W, Kim DW, and Anderson DJ (2014). Antagonistic control of social versus repetitive self-grooming behaviors by separable amygdala neuronal subsets. Cell 158, 1348–1361. 10.1016/j.cell.2014.07.049. [PubMed: 25215491]
10. Unger EK, Burke KJ Jr., Yang CF, Bender KJ, Fuller PM, and Shah NM (2015). Medial amygdalar aromatase neurons regulate aggression in both sexes. Cell Rep 10, 453–462. 10.1016/j.celrep.2014.12.040. [PubMed: 25620703]
11. Nordman JC, Ma X, Gu Q, Potegal M, Li H, Kravitz AV, and Li Z (2020). Potentiation of Divergent Medial Amygdala Pathways Drives Experience-Dependent Aggression Escalation. J Neurosci 40, 4858–4880. 10.1523/JNEUROSCI.0370-20.2020. [PubMed: 32424020]
12. Padilla SL, Qiu J, Soden ME, Sanz E, Nestor CC, Barker FD, Quintana A, Zweifel LS, Ronnekleiv OK, Kelly MJ, and Palmiter RD (2016). Agouti-related peptide neural circuits mediate adaptive behaviors in the starved state. Nat Neurosci 19, 734–741. 10.1038/nn.4274. [PubMed: 27019015]
13. Miller SM, Marcotulli D, Shen A, and Zweifel LS (2019). Divergent medial amygdala projections regulate approach-avoidance conflict behavior. Nat Neurosci 22, 565–575. 10.1038/s41593-019-0337-z. [PubMed: 30804529]

14. Lischinsky JE, Yin L, Shi C, Prakash N, Burke J, Shekaran G, Grba M, Corbin JG, and Lin D (2023). Hardwired to attack: Transcriptionally defined amygdala subpopulations play distinct roles in innate social behaviors. bioRxiv, 2023.2003.2016.532692. 10.1101/2023.03.16.532692
15. Karigo T, Kennedy A, Yang B, Liu M, Tai D, Wahle IA, and Anderson DJ (2020). Distinct hypothalamic control of same- and opposite-sex mounting behaviour in mice. Nature. 10.1038/s41586-020-2995-0.
16. Wei YC, Wang SR, Jiao ZL, Zhang W, Lin JK, Li XY, Li SS, Zhang X, and Xu XH (2018). Medial preoptic area in mice is capable of mediating sexually dimorphic behaviors regardless of gender. Nat Commun 9, 279. 10.1038/s41467-017-02648-0. [PubMed: 29348568]
17. Michael V, Goffinet J, Pearson J, Wang F, Tschida K, and Mooney R (2020). Circuit and synaptic organization of forebrain-to-midbrain pathways that promote and suppress vocalization. Elife 9. 10.7554/eLife.63493.
18. Gao SC, Wei YC, Wang SR, and Xu XH (2019). Medial Preoptic Area Modulates Courtship Ultrasonic Vocalization in Adult Male Mice. Neurosci Bull 35, 697–708. 10.1007/s12264-019-00365-w. [PubMed: 30900143]
19. Knoedler JR, Inoue S, Bayless DW, Yang T, Tantry A, Davis CH, Leung NY, Parthasarathy S, Wang G, Alvarado M, et al. (2022). A functional cellular framework for sex and estrous cycle-dependent gene expression and behavior. Cell 185, 654–671 e622. 10.1016/j.cell.2021.12.031. [PubMed: 35065713]
20. Bayless DW, Yang T, Mason MM, Susanto AAT, Lobdell A, and Shah NM (2019). Limbic Neurons Shape Sex Recognition and Social Behavior in Sexually Naive Males. Cell. 10.1016/j.cell.2018.12.041.
21. Yang B, Karigo T, and Anderson DJ (2022). Transformations of neural representations in a social behaviour network. Nature 608, 741–749. 10.1038/s41586-022-05057-6. [PubMed: 35922505]
22. Zhou X, Li A, Mi X, Li Y, Ding Z, An M, Chen Y, Li W, Tao X, Chen X, and Li Y (2023). Hyperexcited limbic neurons represent sexual satiety and reduce mating motivation. Science 379, 820–825. 10.1126/science.abl4038. [PubMed: 36758107]
23. Jennings KJ, and de Lecea L (2020). Neural and Hormonal Control of Sexual Behavior. Endocrinology 161. 10.1210/endocr/bqaa150.
24. Wu MV, and Shah NM (2011). Control of masculinization of the brain and behavior. Current opinion in neurobiology 21, 116–123. 10.1016/j.conb.2010.09.014. [PubMed: 20970320]
25. Edwards D, and Burge K (1971). Early androgen treatment and male and female sexual behavior in mice. Hormones and Behavior 2, 49–58. 10.1016/0018-506x(71)90037-7.
26. McCarthy MM (2008). Estradiol and the developing brain. Physiol Rev 88, 91–124. 10.1152/physrev.00010.2007. [PubMed: 18195084]
27. Ogawa S, Chester AE, Hewitt SC, Walker VR, Gustafsson JA, Smithies O, Korach KS, and Pfaff DW (2000). Abolition of male sexual behaviors in mice lacking estrogen receptors alpha and beta (alpha beta ERKO). Proc Natl Acad Sci U S A 97, 14737–14741. 10.1073/pnas.250473597. [PubMed: 11114183]
28. Wersinger SR, Sannen K, Villalba C, Lubahn DB, Rissman EF, and De Vries GJ (1997). Masculine sexual behavior is disrupted in male and female mice lacking a functional estrogen receptor alpha gene. Hormones and Behavior 32, 176–183. DOI 10.1006/hbeh.1997.1419. [PubMed: 9454668]
29. Ogawa S, Lubahn DB, Korach KS, and Pfaff DW (1997). Behavioral effects of estrogen receptor gene disruption in male mice. Proc Natl Acad Sci U S A 94, 1476–1481. [PubMed: 9037078]
30. Zha X, Wang L, Jiao ZL, Yang RR, Xu C, and Xu XH (2020). VMHvl-Projecting Vglut1+ Neurons in the Posterior Amygdala Gate Territorial Aggression. Cell Rep 31, 107517. 10.1016/j.celrep.2020.03.081. [PubMed: 32320666]
31. Yamaguchi T, Wei D, Song SC, Lim B, Tritsch NX, and Lin D (2020). Posterior amygdala regulates sexual and aggressive behaviors in male mice. Nature neuroscience 23, 1111–1124. 10.1038/s41593-020-0675-x. [PubMed: 32719562]
32. Stagkourakis S, Spigolon G, Liu G, and Anderson DJ (2020). Experience-dependent plasticity in an innate social behavior is mediated by hypothalamic LTP. Proceedings of the National Academy of Sciences of the United States of America 117, 25789–25799. 10.1073/pnas.2011782117. [PubMed: 32973099]

33. Chen AX, Yan JJ, Zhang W, Wang L, Yu ZX, Ding XJ, Wang DY, Zhang M, Zhang YL, Song N, et al. (2020). Specific Hypothalamic Neurons Required for Sensing Conspecific Male Cues Relevant to Inter-male Aggression. Neuron. 10.1016/j.neuron.2020.08.025.
34. Stagkourakis S, Spigolon G, Williams P, Protzmann J, Fisone G, and Broberger C (2018). A neural network for intermale aggression to establish social hierarchy. Nat Neurosci 21, 834–842. 10.1038/s41593-018-0153-x. [PubMed: 29802391]
35. Soden ME, Miller SM, Burgeno LM, Phillips PEM, Hnasko TS, and Zweifel LS (2016). Genetic Isolation of Hypothalamic Neurons that Regulate Context-Specific Male Social Behavior. Cell Rep 16, 304–313. 10.1016/j.celrep.2016.05.067. [PubMed: 27346361]
36. Chang CH, and Gean PW (2019). The Ventral Hippocampus Controls Stress-Provoked Impulsive Aggression through the Ventromedial Hypothalamus in Post-Weaning Social Isolation Mice. Cell Rep 28, 1195–1205 e1193. 10.1016/j.celrep.2019.07.005. [PubMed: 31365864]
37. Canteras NS, Simerly RB, and Swanson LW (1992). Connections of the posterior nucleus of the amygdala. J Comp Neurol 324, 143–179. 10.1002/cne.903240203. [PubMed: 1430327]
38. Canteras NS, Simerly RB, and Swanson LW (1992). Projections of the ventral premammillary nucleus. Journal of Comparative Neurology 324, 195–212. 10.1002/cne.903240205. [PubMed: 1430329]
39. Mitra SW, Hoskin E, Yudkovitz J, Pear L, Wilkinson HA, Hayashi S, Pfaff DW, Ogawa S, Rohrer SP, Schaeffer JM, et al. (2003). Immunolocalization of estrogen receptor beta in the mouse brain: comparison with estrogen receptor alpha. Endocrinology 144, 2055–2067. 10.1210/en.2002-221069. [PubMed: 12697714]
40. Juavinett AL, Bekheet G, and Churchland AK (2019). Chronically implanted Neuropixels probes enable high-yield recordings in freely moving mice. Elife 8. 10.7554/eLife.47188.
41. Jun JJ, Steinmetz NA, Siegle JH, Denman DJ, Bauza M, Barbarits B, Lee AK, Anastassiou CA, Andrei A, Aydin C, et al. (2017). Fully integrated silicon probes for high-density recording of neural activity. Nature 551, 232–236. 10.1038/nature24636. [PubMed: 29120427]
42. Siegel M, Buschman TJ, and Miller EK (2015). Cortical information flow during flexible sensorimotor decisions. Science 348, 1352–1355. 10.1126/science.aab0551. [PubMed: 26089513]
43. Steinmetz NA, Zatka-Haas P, Carandini M, and Harris KD (2019). Distributed coding of choice, action and engagement across the mouse brain. Nature 576, 266–273. 10.1038/s41586-019-1787-x. [PubMed: 31776518]
44. Allen WE, Chen MZ, Pichamoorthy N, Tien RH, Pachitariu M, Luo L, and Deisseroth K (2019). Thirst regulates motivated behavior through modulation of brainwide neural population dynamics. Science 364, 253. 10.1126/science.aav3932. [PubMed: 30948440]
45. Gunaydin LA, Grosenick L, Finkelstein JC, Kauvar IV, Fenno LE, Adhikari A, Lammel S, Mirzabekov JJ, Airan RD, Zalocusky KA, et al. (2014). Natural neural projection dynamics underlying social behavior. Cell 157, 1535–1551. 10.1016/j.cell.2014.05.017. [PubMed: 24949967]
46. Cui G, Jun SB, Jin X, Pham MD, Vogel SS, Lovinger DM, and Costa RM (2013). Concurrent activation of striatal direct and indirect pathways during action initiation. Nature 494, 238–242. 10.1038/nature11846. [PubMed: 23354054]
47. Kim CK, Yang SJ, Pichamoorthy N, Young NP, Kauvar I, Jennings JH, Lerner TN, Berndt A, Lee SY, Ramakrishnan C, et al. (2016). Simultaneous fast measurement of circuit dynamics at multiple sites across the mammalian brain. Nat Methods 13, 325–328. 10.1038/nmeth.3770. [PubMed: 26878381]
48. Guo Q, Zhou J, Feng Q, Lin R, Gong H, Luo Q, Zeng S, Luo M, and Fu L (2015). Multi-channel fiber photometry for population neuronal activity recording. Biomed Opt Express 6, 3919–3931. 10.1364/BOE.6.003919. [PubMed: 26504642]
49. Lin MZ, and Schnitzer MJ (2016). Genetically encoded indicators of neuronal activity. Nat Neurosci 19, 1142–1153. 10.1038/nn.4359. [PubMed: 27571193]
50. Sych Y, Chernysheva M, Sumanovski LT, and Helmchen F (2019). High-density multi-fiber photometry for studying large-scale brain circuit dynamics. Nat Methods. 10.1038/s41592-019-0400-4.

51. Leroy F, Park J, Asok A, Brann DH, Meira T, Boyle LM, Buss EW, Kandel ER, and Siegelbaum SA (2018). A circuit from hippocampal CA2 to lateral septum disinhibits social aggression. Nature 564, 213–218. 10.1038/s41586-018-0772-0. [PubMed: 30518859]
52. Wong LC, Wang L, D'Amour JA, Yumita T, Chen G, Yamaguchi T, Chang BC, Bernstein H, You X, Feng JE, et al. (2016). Effective Modulation of Male Aggression through Lateral Septum to Medial Hypothalamus Projection. Curr Biol 26, 593–604. 10.1016/j.cub.2015.12.065. [PubMed: 26877081]
53. Xie Z, Gu H, Shang C, Cheng X, Tang Z, Zhan C, Zhang F, and Cao P (2020). Hypothalamic circuits for mechanically-evoked defensive attack.
54. Zelikowsky M, Hui M, Karigo T, Choe A, Yang B, Blanco MR, Beadle K, Gradinaru V, Deverman BE, and Anderson DJ (2018). The Neuropeptide Tac2 Controls a Distributed Brain State Induced by Chronic Social Isolation Stress. Cell 173, 1265–1279 e1219. 10.1016/j.cell.2018.03.037. [PubMed: 29775595]
55. Falkner AL, Wei D, Song A, Watsek LW, Chen I, Chen P, Feng JE, and Lin D (2020). Hierarchical Representations of Aggression in a Hypothalamic-Midbrain Circuit. Neuron. 10.1016/j.neuron.2020.02.014.
56. Zhu Z, Ma Q, Yang H, Miao L, Pan L, Li K, Zhang X, Wu J, Hao S, Lin S, et al. (2020). A Substantia Innominata-midbrain Circuit Controls a General Aggressive State. 10.1101/2020.04.22.047670.
57. Lischinsky JE, and Lin D (2020). Neural mechanisms of aggression across species. Nat Neurosci. 10.1038/s41593-020-00715-2.
58. Lenschow C, and Lima SQ (2020). In the mood for sex: neural circuits for reproduction. Current opinion in neurobiology 60, 155–168. 10.1016/j.conb.2019.12.001. [PubMed: 31901622]
59. Wang L, Talwar V, Osakada T, Kuang A, Guo Z, Yamaguchi T, and Lin D (2019). Hypothalamic Control of Conspecific Self-Defense. Cell Rep 26, 1747–1758 e1745. 10.1016/j.celrep.2019.01.078. [PubMed: 30759387]
60. Canteras NS, Simerly RB, and Swanson LW (1995). Organization of projections from the medial nucleus of the amygdala: a PHAL study in the rat. J Comp Neurol 360, 213–245. 10.1002/cne.903600203. [PubMed: 8522644]
61. Dong HW, and Swanson LW (2004). Projections from bed nuclei of the stria terminalis, posterior division: implications for cerebral hemisphere regulation of defensive and reproductive behaviors. J Comp Neurol 471, 396–433. 10.1002/cne.20002. [PubMed: 15022261]
62. Morali G, Asuncion Pia Soto M, Luis Contreras J, Arteaga M, Gonzalez-Vidal MD, and Beyer C (2003). Detailed analysis of the male copulatory motor pattern in mammals: hormonal bases. Scand J Psychol 44, 279–288. 10.1111/1467-9450.00346. [PubMed: 12914592]
63. Hull EM, and Dominguez JM (2007). Sexual behavior in male rodents. Horm Behav 52, 45–55. 10.1016/j.yhbeh.2007.03.030. [PubMed: 17499249]
64. Pardo-Bellver C, Cadiz-Moretti B, Novejarque A, Martinez-Garcia F, and Lanuza E (2012). Differential efferent projections of the anterior, posteroventral, and posterodorsal subdivisions of the medial amygdala in mice. Front Neuroanat 6, 33. 10.3389/fnana.2012.00033. [PubMed: 22933993]
65. Smith WJ, Stewart J, and Pfaus JG (1997). Tail pinch induces fos immunoreactivity within several regions of the male rat brain: effects of age. Physiol Behav 61, 717–723. 10.1016/s0031-9384(96)00524-0. [PubMed: 9145942]
66. Kollack-Walker S, and Newman SW (1995). Mating and agonistic behavior produce different patterns of Fos immunolabeling in the male Syrian hamster brain. Neuroscience 66, 721–736. [PubMed: 7644033]
67. Dai B, Sun F, Tong X, Ding Y, Kuang A, Osakada T, Li Y, and Lin D (2022). Responses and functions of dopamine in nucleus accumbens core during social behaviors. Cell Rep 40, 111246. 10.1016/j.celrep.2022.111246. [PubMed: 36001967]
68. Gonzalez-Mariscal G, Gomora P, Caba M, and Beyer C (1992). Copulatory analgesia in male rats ensues from arousal, motor activity, and genital stimulation: blockage by manipulation and restraint. Physiol Behav 51, 775–781. 10.1016/0031-9384(92)90115-i. [PubMed: 1594675]

69. Szechtman H, Hershkowitz M, and Simantov R (1981). Sexual behavior decreases pain sensitivity and stimulated endogenous opioids in male rats. Eur J Pharmacol 70, 279–285. 10.1016/0014-2999(81)90161-8. [PubMed: 6262094]
70. Fang Y-Y, Yamaguchi T, Song SC, Tritsch NX, and Lin D (2018). A Hypothalamic Midbrain Pathway Essential for Driving Maternal Behaviors. Neuron 98, 192–207.e110. 10.1016/j.neuron.2018.02.019. [PubMed: 29621487]
71. Mei L, Yan R, Yin L, Sullivan R, and Lin D (2023). Antagonistic Neural Circuits Drive Opposing Behaviors towards the Young in Females. bioRxiv, 2023.2003.2012.532288. 10.1101/2023.03.12.532288
72. Kim DW, Yao Z, Graybuck LT, Kim TK, Nguyen TN, Smith KA, Fong O, Yi L, Koulena N, Pierson N, et al. (2019). Multimodal Analysis of Cell Types in a Hypothalamic Node Controlling Social Behavior. Cell 179, 713–728 e717. 10.1016/j.cell.2019.09.020. [PubMed: 31626771]
73. Vaughn E, Eichhorn S, Jung W, Zhuang X, and Dulac C (2022). Three-dimensional Interrogation of Cell Types and Instinctive Behavior in the Periaqueductal Gray. bioRxiv, 2022.2006.2027.497769. 10.1101/2022.06.27.497769
74. Brookhart JM, and Dey FL (1941). Reduction of Sexual Behavior in Male Guinea Pigs by Hypothalamic Lesions. American Journal of Physiology-Legacy Content 133, 551–554. 10.1152/ajplegacy.1941.133.3.551.
75. Wei D, Osakada T, Guo Z, Yamaguchi T, Varshneya A, Yan R, Jiang Y, and Lin D (2023). A hypothalamic pathway that suppresses aggression toward superior opponents. Nature Neuroscience 26, 774–787. 10.1038/s41593-023-01297-5. [PubMed: 37037956]
76. Newman SW, Parfitt DB, and Kollack-Walker S (1997). Mating-induced c-fos expression patterns complement and supplement observations after lesions in the male Syrian hamster brain.Ann N Y Acad Sci 807, 239–259. [PubMed: 9071355]
77. Kollack SS, and Newman SW (1992). Mating-Behavior Induces Selective Expression of Fos Protein within the Chemosensory Pathways of the Male Syrian-Hamster Brain. Neurosci Lett 143, 223–228. Doi 10.1016/0304-3940(92)90270-H. [PubMed: 1436670]
78. Coolen LM, Peters HJ, and Veening JG (1997). Distribution of Fos immunoreactivity following mating versus anogenital investigation in the male rat brain. Neuroscience 77, 1151–1161. 10.1016/s0306-4522(96)00542-8. [PubMed: 9130794]
79. Kollack-Walker S, and Newman SW (1997). Mating-induced expression of c-fos in the male Syrian hamster brain: role of experience, pheromones, and ejaculations. J Neurobiol 32, 481–501. 10.1002/(sici)1097-4695(199705)32:5<481::aid-neu4>3.0.co;2-1. [PubMed: 9110260]
80. Kondo Y (1992). Lesions of the medial amygdala produce severe impairment of copulatory behavior in sexually inexperienced male rats. Physiology & Behavior 51, 939–943. 10.1016/0031-9384(92)90074-C. [PubMed: 1615054]
81. Fernandez-Fewell GD, and Meredith M (1994). c-fos expression in vomeronasal pathways of mated or pheromone-stimulated male golden hamsters: contributions from vomeronasal sensory input and expression related to mating performance. J Neurosci 14, 3643–3654. [PubMed: 8207479]
82. Motta SC, Guimaraes CC, Furigo IC, Sukikara MH, Baldo MV, Lonstein JS, and Canteras NS (2013). Ventral premammillary nucleus as a critical sensory relay to the maternal aggression network. Proceedings of the National Academy of Sciences of the United States of America 110, 14438–14443. 10.1073/pnas.1305581110. [PubMed: 23918394]
83. Mos J, Kruk M, Van Poel AD, and Meelis W (1982). Aggressive behavior induced by electrical stimulation in the midbrain central gray of male rats. Aggressive Behavior 8, 261–284.
84. Mos J, Lammers J, Van der Poel A, Bermond B, Meelis W, and Kruk M (1983). Effects of midbrain central gray lesions on spontaneous and electrically induced aggression in the rat. Aggressive Behavior 9, 133–155.
85. Beitz AJ (1982). The organization of afferent projections to the midbrain periaqueductal gray of the rat. Neuroscience 7, 133–159. 10.1016/0306-4522(82)90157-9. [PubMed: 7078723]
86. Gobrogge KL, Liu Y, Jia X, and Wang Z (2007). Anterior hypothalamic neural activation and neurochemical associations with aggression in pair-bonded male prairie voles. J Comp Neurol 502, 1109–1122. 10.1002/cne.21364. [PubMed: 17444499]

87. Ferris CF, Melloni RH Jr., Koppel G, Perry KW, Fuller RW, and Delville Y (1997). Vasopressin/serotonin interactions in the anterior hypothalamus control aggressive behavior in golden hamsters. J Neurosci 17, 4331–4340. [PubMed: 9151749]

88. Canteras NS (2002). The medial hypothalamic defensive system: hodological organization and functional implications. Pharmacol Biochem Behav 71, 481–491. 10.1016/s0091-3057(01)00685-2. [PubMed: 11830182]

89. Martinez RC, Carvalho-Netto EF, Amaral VC, Nunes-de-Souza RL, and Canteras NS (2008). Investigation of the hypothalamic defensive system in the mouse. Behav Brain Res 192,185–190. 10.1016/j.bbr.2008.03.042. [PubMed: 18468701]

90. Albert DJ, and Chew GL (1980). The septal forebrain and the inhibitory modulation of attack and defense in the rat. A review. Behav Neural Biol 30, 357–388. 10.1016/s0163-1047(80)91247-9. [PubMed: 7013753]

91. Chen TW, Wardill TJ, Sun Y, Pulver SR, Renninger SL, Baohan A, Schreiter ER, Kerr RA, Orger MB, Jayaraman V, et al. (2013). Ultrasensitive fluorescent proteins for imaging neuronal activity. Nature 499, 295–300. 10.1038/nature12354. [PubMed: 23868258]

92. Mathis A, Mamidanna P, Cury KM, Abe T, Murthy VN, Mathis MW, and Bethge M (2018). DeepLabCut: markerless pose estimation of user-defined body parts with deep learning. Nature neuroscience 21, 1281–1289. 10.1038/s41593-018-0209-y. [PubMed: 30127430]

93. Osborne JE, and Dudman JT (2014). RIVETS: a mechanical system for in vivo and in vitro electrophysiology and imaging. PLoS One 9, e89007. 10.1371/journal.pone.0089007. [PubMed: 24551206]

94. Burgos-Artizzu XP, Dollár P, Lin D, Anderson DJ, and Perona P (2012). Social behavior recognition in continuous video. (IEEE), pp. 1322–1329.

Highlights

- Intruder sex is widely represented in the expanded social behavior network (SBN).
- Mating and fighting evoke distinct activation patterns in the expanded SBN.
- The network functional connectivity increases widely during social action initiation.
- Intromission and ejaculation are accompanied by “dissociated” brain states.

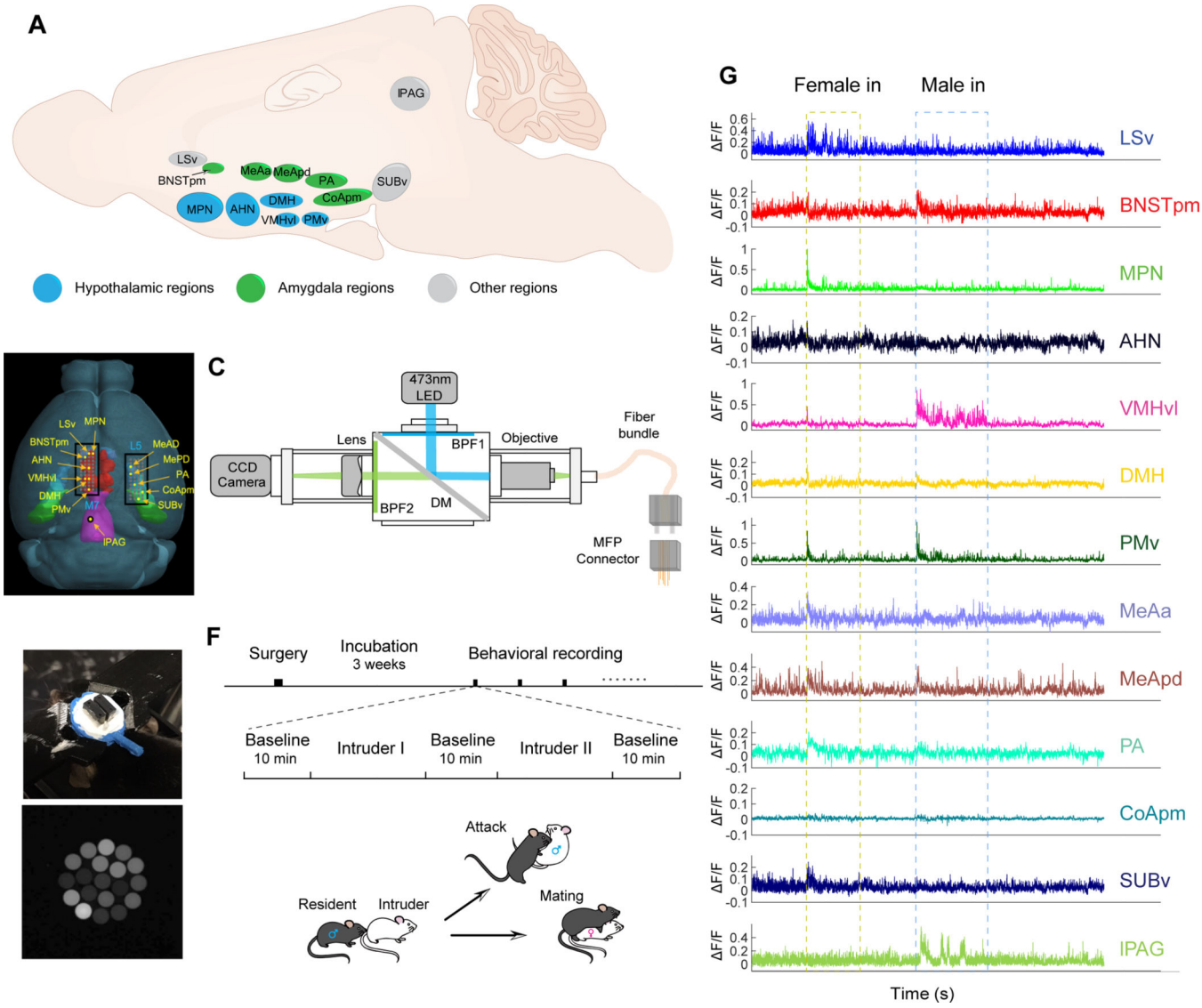

Figure 1: Multi-fiber photometry (MFP) recording of 13 regions in the limbic system.

(A) Illustration showing the recorded regions in the mouse hypothalamus (blue), amygdala (green), and other brain areas (gray).

(B) The optic fiber arrays overlaid on a mouse brain model showing various targeted structures. The model is from https://connectivity.brain-map.org/.

(C) Diagram of the MFP recording system.

(D) An animal with the implanted fiber arrays and a head-fixation ring.

(E) The end of the optic fiber bundle image.

(F) Experimental and each recording session timeline.

(G) Simultaneously recorded GCaMP6f traces (ΔF/F) from a representative recording session.

See also Figures S1-S4.

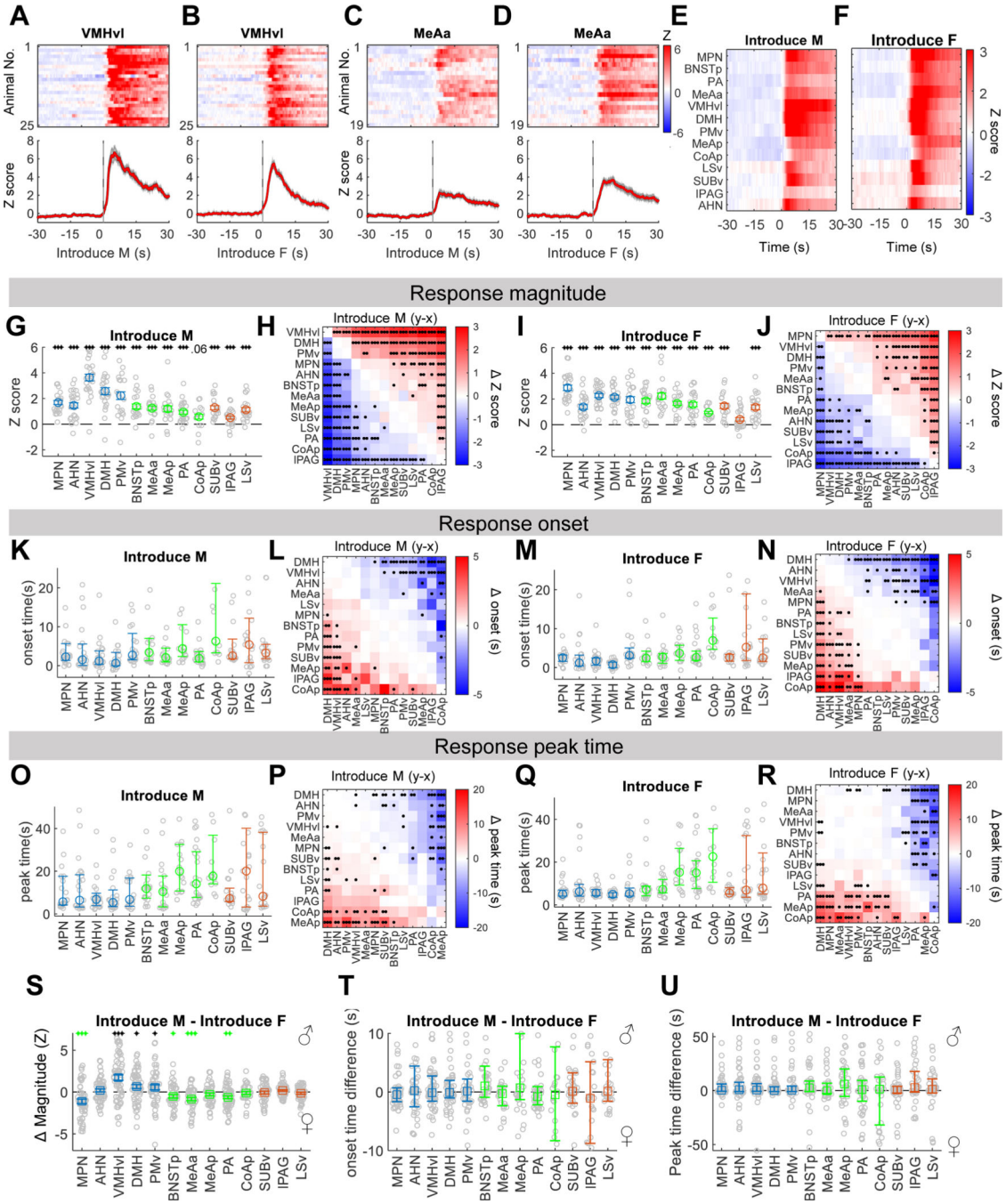

Figure 2: Broad activation of the expanded SBN during initial encounters with male and female intruders.

(A-D) Heatmaps (top) and PETHs (bottom) of Z scored ΔF/F signal of the VMHvl (A, B) and MeAa (C, D) aligned to the male and female intruder introduction from all recording animals.

(E, F) Heatmaps showing average Z-scored ΔF/F aligned to male (E) and female (F) introduction across all recorded regions.

(G, I) Average Z-scored ΔF/F during 0–30s after male (G) and female (I) introduction. n =13–25 animals.

(H, J) Heatmaps showing the difference in average Z-scored ΔF/F during male (H) and female (J) introduction between each pair of regions. n = 21–61 sessions.
(K, M) Average onset of responses upon male (K) and female (M) introduction. n =12-25 animals.
(L, N) Heatmaps showing the difference in average response onset upon male (L) and female (N) introduction between each pair of regions. n = 17–59 sessions.
(O, Q) Average latency to the peak response after male (O) and female (Q) introduction. n =13–25 animals.
(P, R) Heatmaps showing the difference in average response peak time after male (P) and female (R) introduction between each pair of regions. n = 17–59 sessions.
(S, T, U) Differences in response magnitude (Z scored ΔF/F) (S), onset time (T), and peak time (U) during the male and female introduction. n = 28–63 sessions.
Shades in (A-D) and error bars in (G, I, S): Mean ± SEM; in (M, O, Q, T, U): Median ± 25%. Each gray circle in (G, I, K, M, O, Q) represents one animal. Each gray circle in (S-U) represents one recording session. Colored circles in (G, I, K, M, O, Q, S-U) represent the group average. Blue, green, and dark orange indicate hypothalamic regions, amygdala regions, and regions outside the hypothalamus and amygdala, respectively.
(G, I, S, T, U): one sample t-test (if pass Lilliefors normality test) or Wilcoxon signed-rank test (if not pass Lilliefors normality test). (H, J, L, N, P, R): paired t-test (if pass Lilliefors normality test) or Wilcoxon signed-rank test (if not pass Lilliefors normality test). (G-U) p values are adjusted with Benjamini Hochberg procedure for controlling the false discovery rate. *p<0.05; **p<0.01; ***p<0.001. Black: significantly >0; Green: significantly <0; See Table S1 for raw data and detailed statistics.
See also Figures S4-S7 and S14.

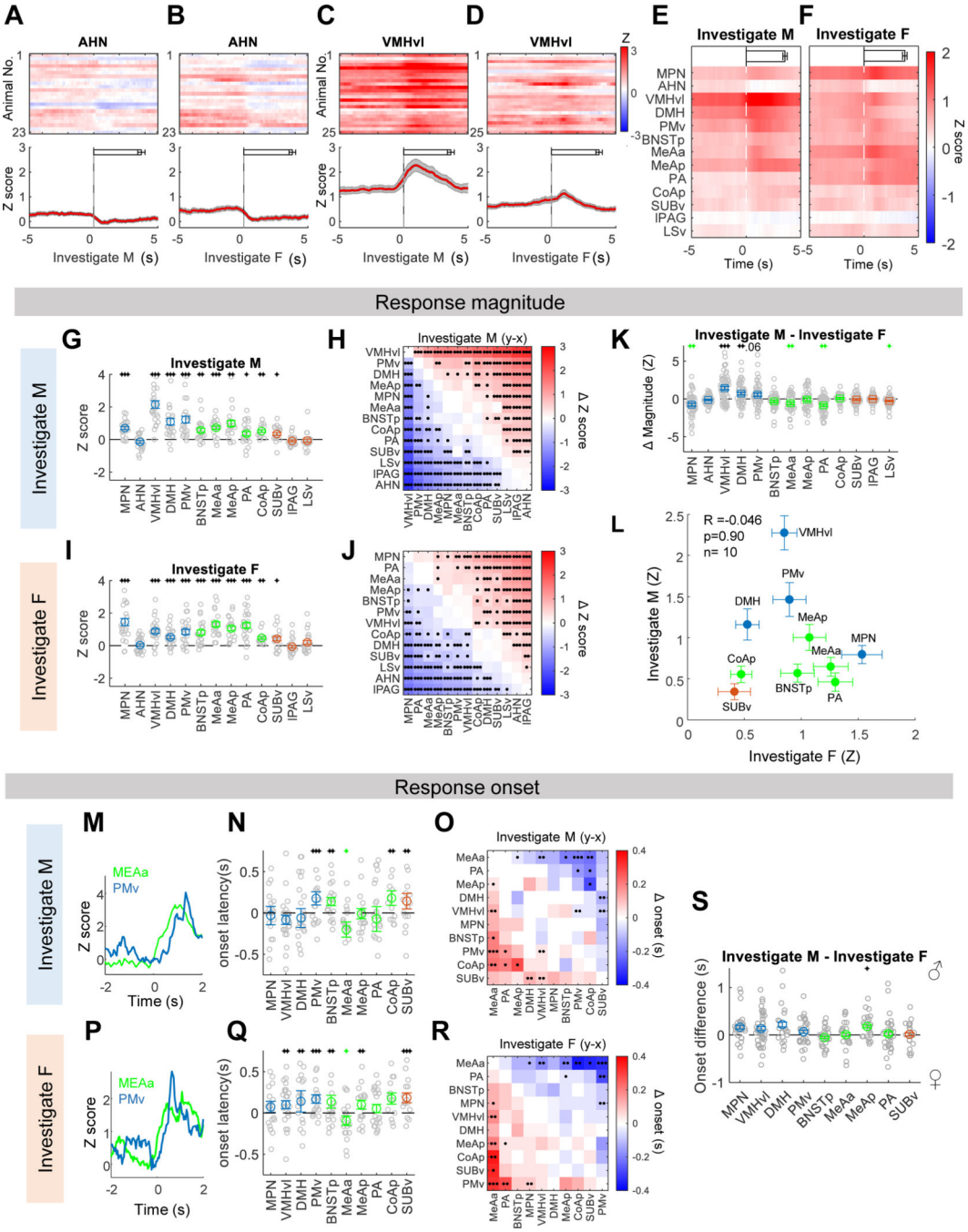

Figure 3: The same regions are activated during male and female investigation but with distinct patterns.

(A-D) Heatmaps (top) and PETHs (bottom) of Z scored ΔF/F signal of the AHN (A-B) and VMHvl (C-D) aligned to the investigation of male (A) and female (B) intruders from all recording animals. Horizontal bars indicate investigation duration (mean ± SEM).

(E-F) Heatmaps showing average Z-scored ΔF/F aligned to the investigation of male (E) and female (F) intruders across all regions. Horizontal bars indicate investigation duration (mean ± SEM).

(G, I) Average Z-scored ΔF/F during the investigation of male (G) and female (I) intruders. n =13–25 animals.

(H, J) Heatmaps showing the difference in average Z-scored ΔF/F during male (H) and female (J) investigation between each pair of regions. n = 19–60 sessions.

(K) Differences in response magnitude (Z-scored ΔF/F) during the male and female investigation. n = 31–59 sessions.

(L) The response magnitude during male and female investigation is uncorrelated. n=10 responsive regions.

(M, P) Representative simultaneously recorded Ca^{2+} traces of MeAa and PMv Esr1 cells during investigating male (M) and female (P) intruders.

(N, Q) The response latency during male (N) and female investigation (Q) of all responsive regions. n = 13–25 animals.

(O, R) Heatmaps showing the difference in average response onset during male (O) and female (R) investigation between each pair of regions. n = 32–345 trials.

(S) Differences in response onset during the male and female investigation. n = 21–39 sessions.

All error bars and shades in PETHs: Mean ± SEM; Each gray circle in (G, I, N, Q) represents one animal. Each gray circle in (K, S) represents one recording session. Colored circles in (G, I, K, L, N, Q, S) represent the group average. Blue, green, and dark orange indicate hypothalamic regions, amygdala regions, and other regions, respectively.

(G, I, K, N, Q, S) one sample t-test (if pass Lilliefors normality test) or Wilcoxon signed-rank test (if not pass Lilliefors normality test). (H, J, O, R) paired t-test (if pass Lilliefors normality test) or Wilcoxon signed-rank test (if not pass Lilliefors normality test). (G-K, N, O, Q-S) p values are adjusted with Benjamini Hochberg procedure for controlling the false discovery rate. *p<0.05; **p<0.01; ***p<0.001. Black: significantly >0; Green: significantly <0; L: Pearson’s cross-correlation. See Table S1 for raw data and detailed statistics.

See also Figures S4-S7 and S14.

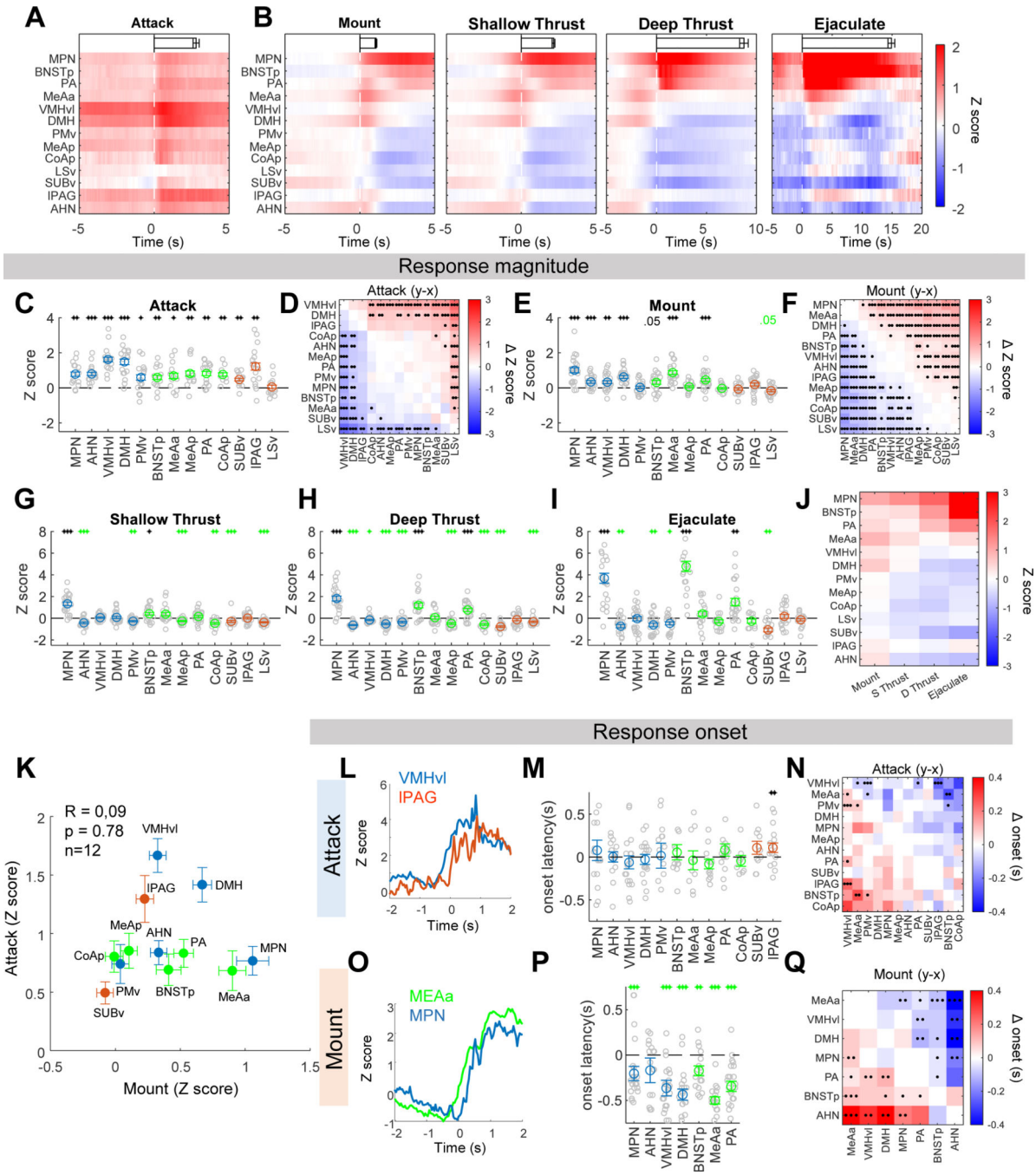

Figure 4: Distinct activation patterns in the expanded SBN during male aggressive and sexual behaviors.

(A-B) Heatmaps showing average Z scored ΔF/F aligned to attack (A) and various phases of sexual behaviors (B) across all recorded regions. Horizontal bars indicate the average duration of the behavior episodes (mean ± SEM).

(C, E) Average Z scored ΔF/F during attack (C) and mount (E). n =8–24 animals.

(D, F) Heatmaps showing differences in average Z scored ΔF/F during attack (D) and mount (F) between each pair of regions. n = 11–55 sessions.

(G-I) Average Z scored ΔF/F during shallow thrust (G), deep thrust (H), and ejaculation (I). n =12–25 animals.

(J) The average Z scored ΔF/F during various stages of male sexual behaviors across regions.

(K) The response magnitude during attack and mount is uncorrelated. n=12 regions that are responsive during at least one behavior.

(L, O) Representative simultaneously recorded Ca2+ traces of VMHvl and lPAG Esr1 cells during attack (L) and MeAa and MPN Esr1 cells during mount (O).

(M, P) The response latency during attack (M) and mount (P) of responsive regions. n = 8–23 animals.

(N, Q) Heatmap showing the difference in average response onset during attack (N) and mount (Q) between each pair of regions. n = 23–260 trials.

All error bars and shades of PETHs: Mean ± SEM; Each gray circle in (C, E, G, H, I, M, and P) represents one animal. Colored circles in (C, E, G, H, I, K, M, and P) represent the group average. Blue, green, and dark orange indicate hypothalamic regions, amygdala regions, and other regions, respectively.

(C, E, G-I, M, P) one sample t-test (if pass Lilliefors normality test) or Wilcoxon signed-rank test (if not pass Lilliefors normality test). (D, F, N, and Q) paired t-test (if pass Lilliefors normality test) or Wilcoxon signed-rank test (if not pass Lilliefors normality test). (C-I, M, N, P, Q) p values are adjusted with Benjamini Hochberg procedure for controlling the false discovery rate. *p<0.05; **p<0.01; ***p<0.001. Black: significantly >0; Green: significantly <0; I: Pearson's cross-correlation. See Table S1 for raw data and detailed statistics.

See also Figures S4, S6, S7 and S14.

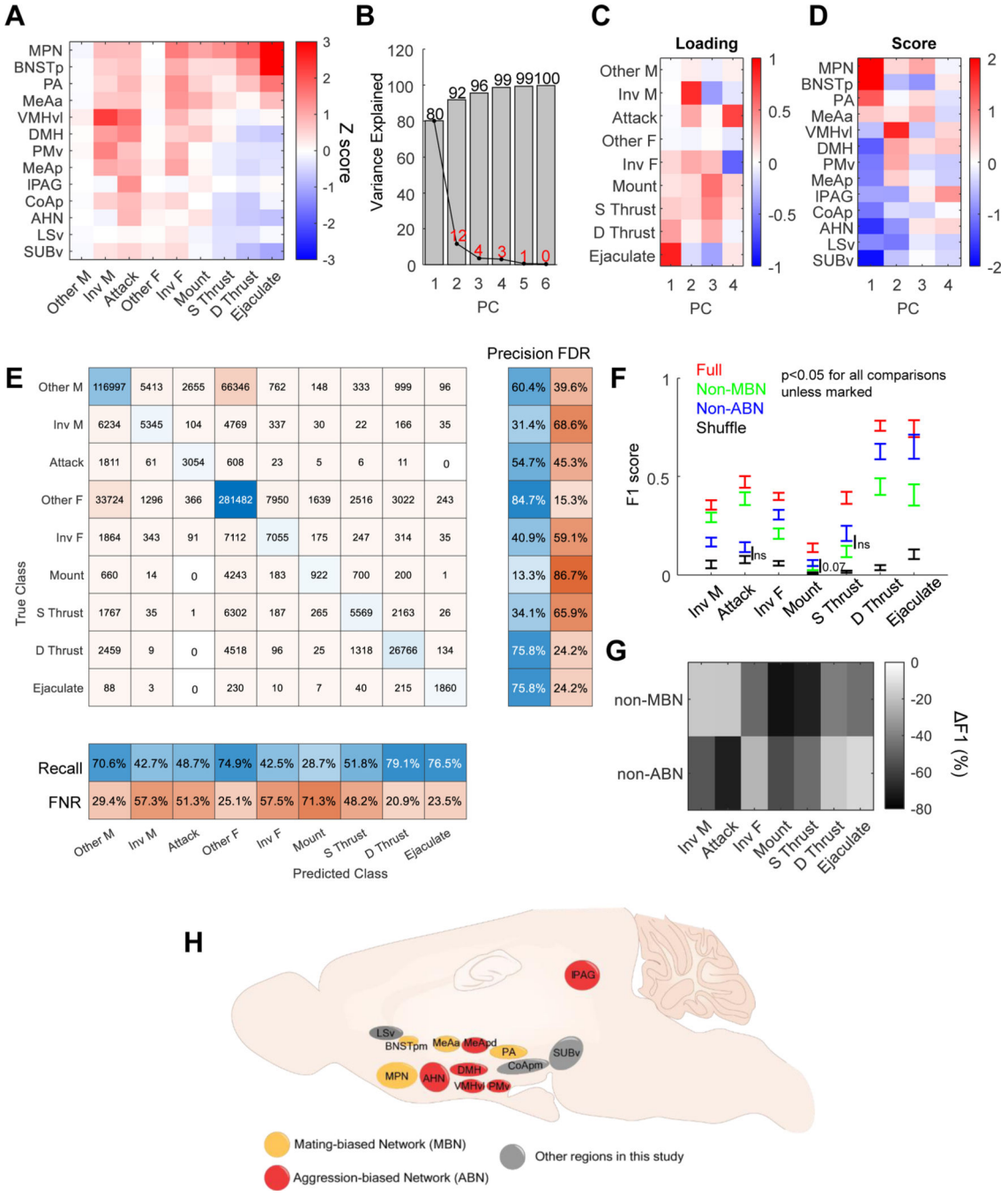

Figure 5. Activities in MBN and ABN predict male sexual and aggressive behaviors, respectively.

(A) Heat map showing the average Z scored ΔF/F during male- and female-directed social behaviors across regions in male mice. “Other M” and “Other F” refer to periods when the male or female intruder is present, but no specific social behavior is annotated. Inv: investigate; S Thrust: shallow thrust; D Thrust: deep thrust.

(B) The variance in responses during different behaviors explained by the first 6 PCs.

(C) The loading (coefficient) of the first 4 PCs.

(D) The scores of the first 4 PCs for each region.

(E) Confusion matrix shows the number of frames that are correctly and incorrectly classified for each behavior across all sessions. Left columns show the precision (blue) and false discovery rate (FDR, orange). Bottom rows show the recall (blue) and false negative rate (FNR, orange).

(F) F1 scores of various behaviors computed using full models that include data from all recording regions, non-MBN models, non-ABN models, and models built with time-shifted data. Error bar: mean ± SEM. Paired t-test (if pass Lilliefors normality test) or Wilcoxon signed-rank test (if not pass Lilliefors normality test). All comparisons have p values < 0.05 unless marked. ns: not significant. n = 17–24 animals.

(G) Heatmap showing the averaged decrease in F1 score when using non-MBN and non-ABN models compared to the full model.

See Table S1 for raw data and detailed statistics.

See also Figure S8 and S14.

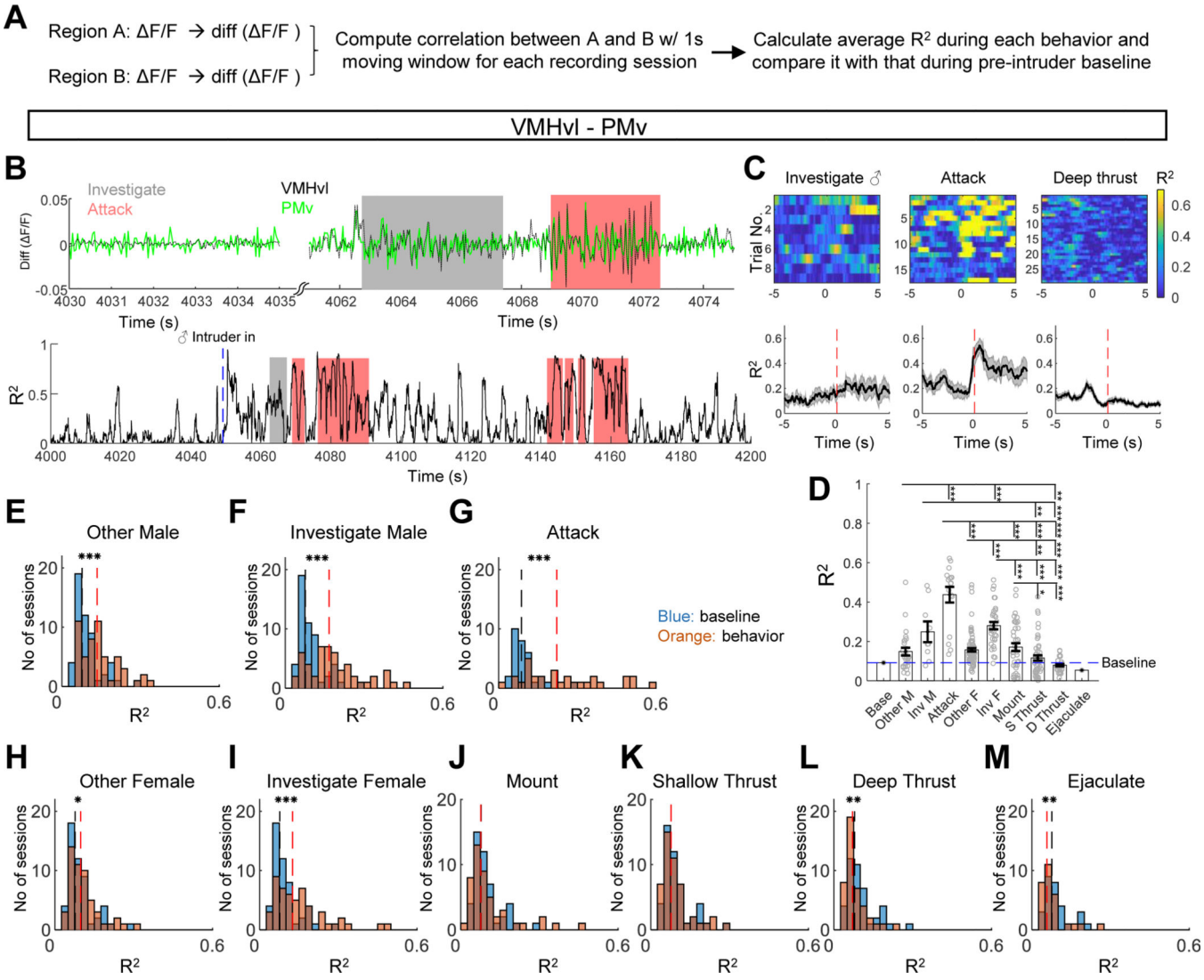

Figure 6. Changes in the VMHvl and PMv functional connectivity during social behaviors.

(A) The procedure to calculate R^2 between a pair of regions during various behaviors.

(B) Differential Z scored ΔF/F traces of VMHvl (black) and PMv (green) (top) and their moment-to-moment R^2 (bottom) from a representative recording session. Shades indicate behavior episodes.

(C) Heatmaps (top) and PETHs (bottom) aligned to the onset of male investigation (left), attack (middle), and deep thrust (right). It is from the same recording session shown in B.

(D) Average R^2 between VMHvl and PMv during various behaviors in the recording session shown in (B, C). n = 1–86 trials. Base: pre-intruder period. Other: With intruder but no specific social behaviors. Inv: investigate; S Thrust: shallow thrust; D Thrust: deep thrust. Kruskal-Wallis test followed by Benjamini Hochberg procedure for controlling the false discovery rate.

(E-M) The distribution of R^2 at the pre-intruder baseline (orange) and during specific behavior epochs (blue). Black and red dashed lines indicate the median values of the R^2 during the baseline and behavior periods. Baseline and behavior sessions are matched.

Paired t-test (if pass Lilliefors normality test) or Wilcoxon signed-rank test (if not pass Lilliefors normality test).

Error bars and shades of PETHs: Mean ± SEM. *p<0.05; **p<0.01; ***p<0.001. See Table S1 for raw data and detailed statistics.

See also Figure S9.

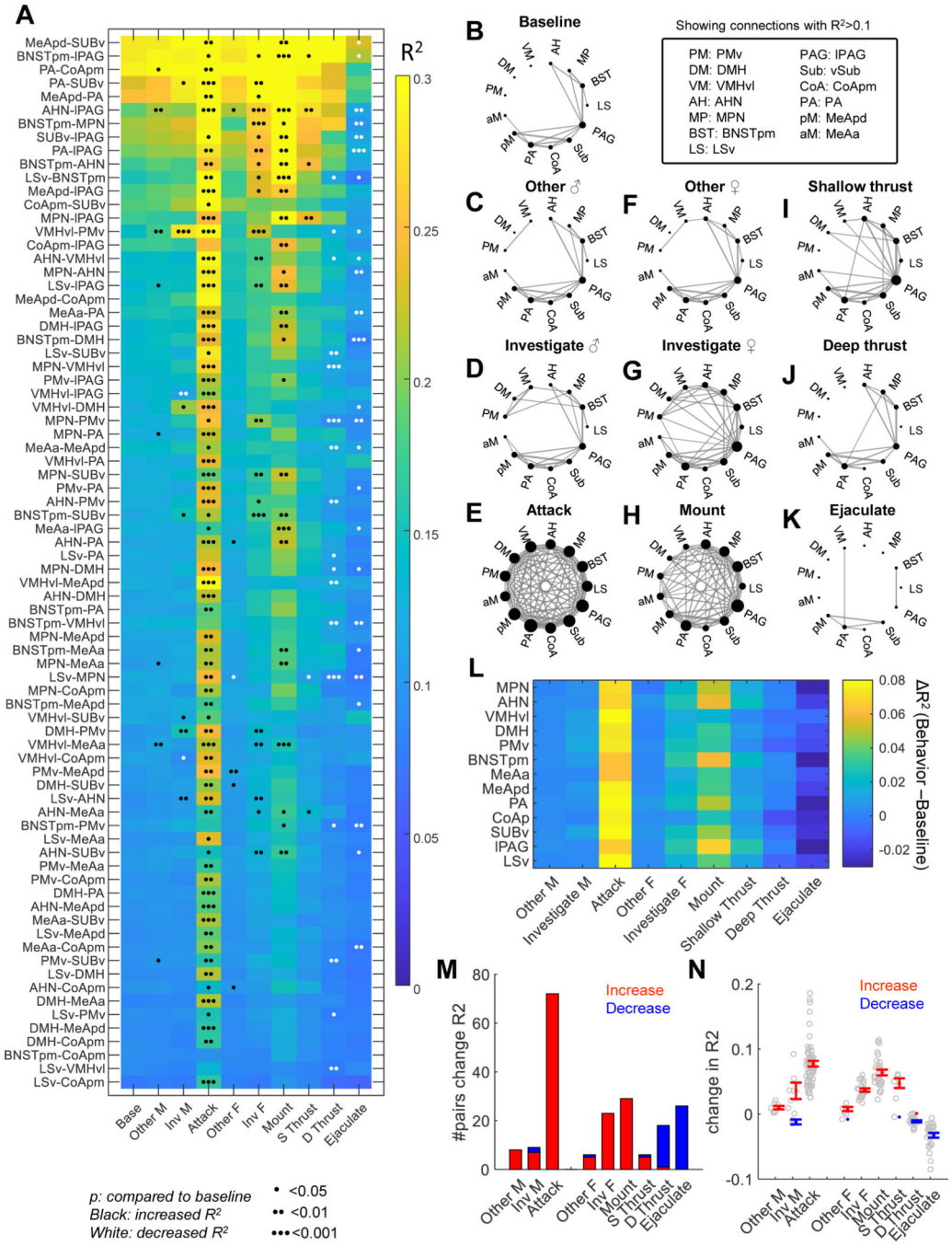

Figure 7. Changes in functional connectivity across the expanded SBN during social behaviors.

(A) Heatmap shows the average R^2 of all pairs of regions during various behavior epochs and its comparison to the R^2 values during the baseline period. Base: pre-intruder period. Other: with intruder but no specific social behaviors. Inv: investigate; S Thrust: shallow thrust; D Thrust: deep thrust. Paired t-test (if pass Lilliefors normality test) or Wilcoxon signed-rank test (if not pass Lilliefors normality test). p values are adjusted using with Benjamini Hochberg procedure for controlling the false discovery rate. *q<0.05;

**q<0.01; ***q<0.001. Black and white: significantly increase and decrease from baseline, respectively.

(B-K) Graph plots showing the strength of functional connectivity (R^2) among different regions during various social behavior epochs. Only connections with R^2> 0.1 are shown. The size of a node reflects its overall connection strength.

(L) The averaged change of R^2 of each region with all other regions during various behaviors.

(M) The number of pairs of regions that show significantly increased R^2 (red) or decreased R^2 (blue) from the pre-intruder baseline.

(N) Change in R2 values from the pre-intruder baseline for significantly changed connections. Red and blue show the mean ± SEM of significantly increased and decreased connections during each behavior. n = 0–72 pairs of regions.

See Table S1 for raw data and detailed statistics.

See also Figures S10-S14.

KEY RESOURCES TABLE

REAGENT or RESOURCE	SOURCE	IDENTIFIER
Bacterial and Virus Strains		
AAV1-CAG-Flex-GCaMP6f-WPRE.SV40	Chen et al.[91]	Addgene #100835-AAV1
AAV2-CAG-FLEX-GCaMP6f-WPRE.SV40	Chen et al.[91]	Vigene Biosciences, Custom
Experimental Models: Organisms/Strains		
Esr1-Cre mice	Lee et al.[6]	Jackson lab, Strain No. 017911
Deposited data		
Multi-fiber recording dataset	This study	10.5281/zenodo.8128564
Software and Algorithms		
MATLAB R2021a	MathWorks	https://www.mathworks.com/products/matlab.html; RRID:SCR_001622
Prism 9	GraphPad Software	https://www.graphpad.com/scientific-software/prism/; RRID:SCR_002798
StreamPix 5	NorPix	https://www.norpix.com/products/streampix/streampix.php; RRID:SCR_015773
Body tracking code	Lin et al.[8]	https://github.com/pdollar/toolbox
DeepLabCut	Mathis et al.[92]	https://github.com/DeepLabCut/DeepLabCut RRID:SCR_021391
MFP analysis code	This study	10.5281/zenodo.8128564